Exploring minijets beyond the leading power

P. Kotko, A. M. Stasto, and M. Strikman

Exploring minijets beyond the leading power

P. Kotko, A.M. Stasto, M. Strikman

Department of Physics, The Pennsylvania State University

University Park, PA 16802, United States

Abstract

The crucial parameter in the current Monte Carlo models of high energy hadron-hadron interaction is the transverse momentum cutoff p_{T0} for parton-parton interactions which slowly grows with energy and regularizes the cross section. This modification of the collinear factorization formula goes beyond the leading power and thus a natural question arises if such cutoff can be extracted from a formalism which takes into account power corrections. In this work, we consider the High Energy Factorization (HEF) valid at small x and a new model, based on a similar principle to HEF, which in addition has a limit respecting the Dokshitzer-Dyakonov-Troyan formula for the dijet momentum disbalance spectrum. Minijet cross section and its suppression is then analyzed in two ways. First, we study minijets directly in the low-p_T region, and demonstrate that higher twist corrections do generate suppression of the inclusive jet production cross section though these effects are not leading to the increase of the cutoff with incident energy. Second, we consider hard inclusive dijet production where Multi Parton Interactions (MPIs) with minijets produce power corrections. We introduce an observable constructed from differential cross section in the ratio τ of dijet disbalance to the average dijet p_T and demonstrate that the $\tau > 1$ region is sensitive to the cutoff p_{T0} in the MPI minijet models. The energy dependence of the cutoff is reflected in the energy dependence of the bimodality coefficient b of the τ distribution. We compare b calculated from pythia, where one can conveniently control MPIs by the program parameters, and HEF for a few unintegrated gluon distributions (UGDs). We find that the energy dependence of b is very sensitive to the particular choice of UGD and in some models it resembles predictions of the Monte Carlo models.

1 Introduction

The rise of the total cross section in hadron-hadron collisions with energy is driven by *minijets*, i.e. jets with relatively low transverse momenta p_T, of the order of a few GeV. From the QCD point of view, this growth is attributed to the rise of the parton density inside a hadron with decreasing value of longitudinal momentum x (or increasing CM energy of the collision). At leading order (LO) the colliding partons (mostly gluons at high energies) produce two final state partons and give rise to two jets. The problem is, however, that the resulting QCD expression is divergent when $p_T \to 0$. This is of course not a paradox, simply the very low p_T region is out of the applicability of the formalism operating on partons (i.e. collinear factorization theorem [1], see Section 2.1). Thus one has to introduce a cutoff, $p_{T\,min}$, above which the formula makes sense [2]. This is the starting point for so-called minijet models and models including Multi Parton Interactions (MPIs) which are at the heart of modern event generators like pythia [3] or herwig $++$ [4]. The basic idea is that since the minijet cross section $\sigma_{minijet}(p_{T\,min})$ can easily

exceed the total cross section σ_{tot} (for low values of $p_{T\min}$), the ratio $\sigma_{\text{minijet}}/\sigma_{\text{ND}}$, with σ_{ND} being a non-diffractive inelastic component of the total cross section, gives an average number of hard binary collisions per event, i.e. MPI events [5]. The $p_{T\min}$ is a free parameter of the model. Typically, one does not implement the sharp cutoff but rather a smooth transition regulated by another parameter p_{T0}. Comparison of the models with MPI with the data indicates that hadron production at small impact parameters grows in these models too fast with increase of $\sqrt{S}$. Also the cross section of the interaction at large impact parameters grows faster than indicated by the data on profile function of the pp interaction leading to cross section much larger than the experimental one [6, 7]. The typical resolution is to let the p_{T0} parameter to be energy dependent $p_{T0} = p_{T0}\,(S)$, slowly growing with S.

We see that there are two general features of the minijet models: (i) an existence of a scale p_{T0} above which perturbative collinear factorization applies and (ii) the MPI-type events. Let us note, that in a typical minijet model these features are related in the sense that the MPI models require the property (i), which in turn, on itself, can be viewed as a consequence of color confinement [5] and is independent on MPIs. However at the LHC energies one needs a cutoff on the scale of $3\,\text{GeV}$ and growing with S, making it unlikely that the cutoff could be solely non-perturbative effect. On the other hand, the MPIs became a separate branch of high energy physics, not necessarily related to minijets. For example one of the typical direct MPI signals is expected to be a four-jet hard event with back-to-back dijets [8]. On the theory side the MPI physics is a very complicated subject and most often is restricted to the double parton scattering (DPS), see [9] for a comprehensive review. So far no proof exists of the QCD factorization theorem for DPS, although recently a progress has been made towards the proof of DPS in the double Drell-Yan process [10].

In this work we have undertaken an attempt to understand the origin of the cutoff and the low p_T suppression within the perturbative QCD. As we will discuss later, the application of the cutoff to the collinear factorization formula extends it beyond the leading power. Thus, any approach which aims to explain the cutoff has to incorporate higher twists. Non-negligible power corrections may be generated by large transverse momenta of incoming partons entering the hard collision, as compared to the hard scale of the process. These features are naturally incorporated in the High Energy Factorization (HEF) (or k_T-factorization) approaches [11–15]. There, the transverse momentum of the dijet pair is no longer zero, but equals to the sum of the transverse momenta of the incoming off-shell gluons. The distribution of these gluons in longitudinal and transverse momenta is given by so-called Unintegrated Gluon Distribution (UGD). Thus, in principle, the cutoff on the jet p_T is related to the behavior of UGDs in transverse momentum which, in the low x limit, is given by Balitsky-Fadin-Kuraev-Lipatov (BFKL) equation [16–18] or some BFKL-type evolution. Furthermore, the gluon emissions with small transverse momenta are suppressed by the Sudakov form factor. In fact, for some UGD models [19, 20] the transverse momentum of the gluons is generated by the Sudakov form factor and the standard Dokshitzer-Gribov-Lipatov-Altarelli-Parisi (DGLAP) evolution. This is somewhat similar to the soft gluon resummation [21] technique which was used in [22, 23] to build an eikonal minijet model which does not require a cutoff (but it is suitable only for the total cross section).

The strategy for our paper is as follows. Using the HEF for inclusive dijet production we shall perform two independent studies of the p_T cutoff:

Study 1. A direct study, where we calculate the p_T spectrum for $p_T \gtrsim 2\,\text{GeV}$ and see if there is a suppression and determine its energy dependence.

Study 2. An indirect study, where we analyze the hard dijet production with $p_T \gtrsim 25\,\text{GeV}$ and look for an observable which is sensitive to power corrections which would come from

MPIs in minijet models.

As for the study 1, the issue of a direct access to the p_T cutoff within an approach involving an internal k_T is actually known in the literature. In [24] it was shown that indeed such approach can produce p_T suppression, which has roughly the correct energy dependence. There is however an important difference to our study 1. We use HEF of [12–15] which factorizes the cross section into UGD and a genuine $2 \rightarrow 2$ off-shell hard process which extends collinear minijet formula beyond leading power. In [24] the minijet production was considered in the sense of a chain of emissions which does not have hard $2 \rightarrow 2$ process. It is rather suitable for constructing shower-like Monte Carlo program [25] that can be used to study particle production [26]. More precisely, in [24] the authors considered a modification of the Catani-Ciafaloni-Fiorani-Marchesini (CCFM) [27–29] evolution, so-called linked dipole chain model [30], in which any emission in the chain can contribute a minijet (the emissions are unordered in transverse momenta and thus following this logic any sub-collision in the chain can be considered as 'hard'). On the contrary, in HEF, we require that the large enough hard scale is present that distinguishes the hard $2 \rightarrow 2$ process from the chain of remaining emissions. Since this hard scale is identified with the jet p_T the two directly emitted partons should be actually considered as hard jets, not the minijets. In the first approximation hard jets are produced back-to-back and described by the leading power collinear approach, which does not feature any suppression factor. We will see this feature in our calculations when we compute the p_T spectra in the small p_T region from HEF. That is, we will find no suppression in the p_T spectra of the type present in the minijet models. Nonetheless, it does not mean that there are no minijets in HEF. In fact, HEF takes into account additional emissions visible as the jet imbalance, and thus as power corrections.

The above motivates the study 2, which concentrates on the indirect access to minijets in HEF. We introduce an observable related to the dijet imbalance K_T, which is sensitive to minijets. Specifically, we shall consider the cross section differential in the ratio τ, of K_T to the dijet average p_T. We will check actual sensitivity of this observable on minijets, in particular on p_{T0} cutoff, using pythia and then we shall compare them to similar calculations in HEF models. Next, we introduce bimodality coefficient which characterizes the τ spectrum. We observe that the energy dependence of this coefficient is very sensitive to the particular minijet model. We will see that some of the UGDs used in HEF give energy dependence similar to the one coming from the minijet models in pythia. This would then indirectly confirm the statement from [24], but in a way that can be confirmed experimentally when such observable is measured.

Our work is organized as follows. In Section 2 we systematically review theory behind minijets. First, in Subsection 2.1 we review the collinear factorization for the minijet production and then, in Subsection 2.2, we describe in details how the cutoff is introduced. In Subsection 2.3 we review the HEF and discuss its relevance to minijet cross section. In particular, we shall explain that the leading twist limit of HEF does not reproduce the result of Dokshitzer-Dyakonov-Troyan (DDT) [31] for the dijet momentum disbalance. Therefore, in the next Subsection 2.4 we construct a model similar to HEF but having the DDT limit. In the following sections we will turn to numerical simulations. First, in Section 3 we shall describe in some details the process under consideration, kinematic cuts, etc. in order to unambiguously define the observables. Later, in Section 4 we will analyze the inclusive dijet spectra in the low p_T region in order to see whether the suppression is produced in HEF and the DDT-based model we constructed in Subsection 2.4 (study 1). Finally, in Section 5 we will turn to hard inclusive dijets and study the minijets as a power correction (study 2). We will summarize and make our conclusions in Section 6.

2 Minijets in selected approaches

2.1 Collinear factorization and soft gluon resummation

The starting point for a typical minijet model is the collinear factorization formula, which how-ever has to be modified. In this introductory section we review this issue in a more quantitative way.

The QCD collinear factorization theorem (see e.g. [1] for a review) expresses the cross section for *hard* dijet production as

$$\sigma_{2\text{jet}} = \sum_{a,b} \int \frac{dx_A}{x_A} \frac{dx_B}{x_B} \, d\hat{\sigma}_{ab}\left(x_A, x_B; \mu^2\right) f_{a/A}\left(x_A; \mu^2\right) f_{b/B}\left(x_B; \mu^2\right) + \mathcal{O}\left(\frac{\mu_0^2}{\mu^2}\right), \quad (1)$$

where $f_{a/A}$, $f_{b/B}$ are integrated parton distribution functions (PDFs) for a parton a, b inside a hadron A, B, and $d\hat{\sigma}_{ab}$ is a partonic, fully differential, cross section which can be calculated order by order in perturbation theory. In general the partons a, b can be quarks and gluons, including heavy quarks. The phase space cuts necessary to define a jet cross section (i.e. a suitable jet algorithm) are hidden inside the partonic cross section. The hard scale μ is the largest scale in the problem and is typically taken to be the average transverse momentum of the jets, $P_T = \left(|\vec{p}_{T1}| + |\vec{p}_{T2}|\right)/2$. The remainder, i.e. the higher 'twist' corrections in (1) are suppressed by the powers of the ratio μ_0^2/μ^2, where μ_0 is the largest of some other scales present in the problem, e.g. heavy quark masses, dijet disbalance, etc.

Since the purpose of this work is to study minijets, let us restrict to the semi-hard jets having transverse momenta $p_T \gtrsim 2\,\text{GeV}$. In addition, we are interested in the total CM energies being much larger than this scale. For such regime the factorization theorem (1) starts to fail. Two major sources for this are various large logs (containing ratios of very different scales) and power corrections which are no longer small.

Certainly, the formula (1) would be perfectly valid for fixed s and $\mu^2 \to \infty$, but obviously this is not the case for minijets. In order to illustrate the problems more quantitatively, let us consider a cross section (1) as a function of the disbalance between the jets, K_T^2, when $\mu_0^2 \ll K_T^2 \ll \mu^2$. To leading logarithmic accuracy it is given by the formula due to Dokshitzer-Dyakonov-Troyan, the so-called 'DDT formula'[1] [31]

$$\frac{d\sigma_{2\text{jet}}}{dK_T^2} = \sum_{a,b,c,d} \int \frac{dx_A}{x_A} \frac{dx_B}{x_B} \, d\hat{\sigma}_{ab \to cd}\left(x_A, x_B; \mu^2\right)$$

$$\times \frac{\partial}{\partial K_T^2} \left\{ f_{a/H}\left(x_A; K_T^2\right) T_a\left(K_T^2, \mu^2\right) f_{b/H}\left(x_B; K_T^2\right) T_b\left(K_T^2, \mu^2\right) T_c\left(K_T^2, \mu^2\right) T_d\left(K_T^2, \mu^2\right) \right\}$$

$$+ \mathcal{O}\left(\frac{K_T^2}{\mu^2}\right), \quad (2)$$

where $T_a\left(\mu_1^2, \mu_2^2\right)$ is a 'Sudakov' form factor for a parton a (for the original Sudakov's form factor in QED see [32]). It can be thought of as a probability for the parton a to evolve between the scales μ_1 and μ_2 without any resolvable emissions. We shall give the explicit formula later (see Subsection 2.4, Eq. (33)), for now let us just mention that

$$T_a\left(\mu^2, \mu^2\right) = 1, \quad T_a\left(\mu_0^2, \mu^2\right) \simeq 0, \quad \mu \gg \mu_0, \quad (3)$$

---

[1]More precisely, the notion 'DDT formula' refers to the factorization formula for the transverse distribution of the Drell-Yan pairs in hadron-hadron collision. Its generalization for decorrelation of a di-hadron system in hadron-hadron collision was given in [31]. In the present work we use the term 'DDT formula' for the latter.

for μ_0 being the lowest scale in our problem. Let us remark, that the relevant DDT formula in [31] was actually derived for a production of hadrons in hadron-hadron collision, and thus it contained fragmentation functions which accompanied the form factors T_c, T_d in (2). For the purpose of this paper we have adjusted that formula for dijets by setting the fragmentation functions to be the delta functions. Let us note, that due to the listed properties of the Sudakov form factors, this formula reduces to (1) when integrated over the jet disbalance K_T. Since the appearance of the DDT formula a lot of effort has been put into improving the accuracy of perturbative predictions for such semi-inclusive observables. In particular so-called Transverse Momentum Dependent (TMD) factorization theorem has been established for certain processes [1]. We shall discuss these at the end of this section and for the purpose of the present discussion we shall stick to the leading-log formula (2).

In case of minijets, the formula (2) looses its accuracy as now K_T can be easily of the order of μ (which is the average p_T of the jets). This can be seen by inspecting the derivative in (2) as a function of K_T, for example in the pure gluonic channel:

$$G\left(x, K_T^2, \mu^2\right) = \frac{\partial}{\partial K_T^2} \left\{ f_{g/H}^2 \left(x; K_T^2\right) T_g^4 \left(K_T^2, \mu^2\right) \right\} . \tag{4}$$

This distribution is plotted in Fig. 1 as a function of K_T for fixed $\mu = P_T = 2.5\,\mathrm{GeV}$ and $\mu = 300\,\mathrm{GeV}$, and two values of x (note that for simplicity we have used the same values of x entering both PDFs in (4)). In this presentation we use the leading order GRV98 PDF set [33] (we explain the reason for using this PDF set in Section 3). We see that the characteristic K_T, let us call it K_{T0}, generated by the density G is large when compared to the average P_T of minijets so that $K_{T0}/P_T \sim \mathcal{O}(1)$ (left plot in Fig. 1; K_{T0} may be defined for example as the value for which the distribution has a maximum, although median would probably be a more realistic estimate). For comparison, we plot the same distribution for hard jets (right plot in Fig. 1) with $\mu = 300\,\mathrm{GeV}$. For the latter, the ratio K_{T0}/P_T becomes much smaller than the unity and the situation improves with increasing scale. To summarize, the power corrections cannot be neglected for minijets and one has to necessarily venture beyond leading 'twist' to account for minijets. Let us remind, that the formula (2) is a more 'exclusive' version of (1) and the condition that we can neglect the power corrections is actually a condition necessary to obtain (1) when the integral over K_T is performed.

There is yet another source of errors in the DDT formula, namely the sub-leading logs. Actually, in its original formulation the DDT formula was written for processes with only two hadrons such as for instance the Drell-Yan process [34]. Assuming strong ordering in the transverse momenta of emitted gluons one obtains a formula similar to (2) but with two Sudakov form factors instead of four (and of course with an appropriate hard partonic cross section relevant to Drell-Yan process). However, the strong ordering in transverse momenta for the soft gluons is a too strong assumption and gives a non-physical suppression in the low K_T limit. The improved approach for Drell-Yan pairs was proposed in [21, 35, 36] which resums the soft gluons (thus the approach is often called the 'soft gluon resummation') using the impact parameter space conjugate to transverse momenta. As a result one finds a flat distribution at small K_T rather than an exponentially suppressed cross section. There exists a more general approach, so called Transverse Momentum Dependent (TMD) factorization (see e.g. [1]). It is a rigorous factorization theorem of QCD and is valid to leading power in the hard scale. It is important to note, that this theorem is valid for processes with at most two hadrons. Thus the most complicated processes are Drell-Yan process [37] and semi-inclusive deep inelastic scattering [38]. The theorem is violated when more hadrons are present [39], thus it fails for example for jet production in hadron-hardon collision. However, although the TMD factorization is not a strict
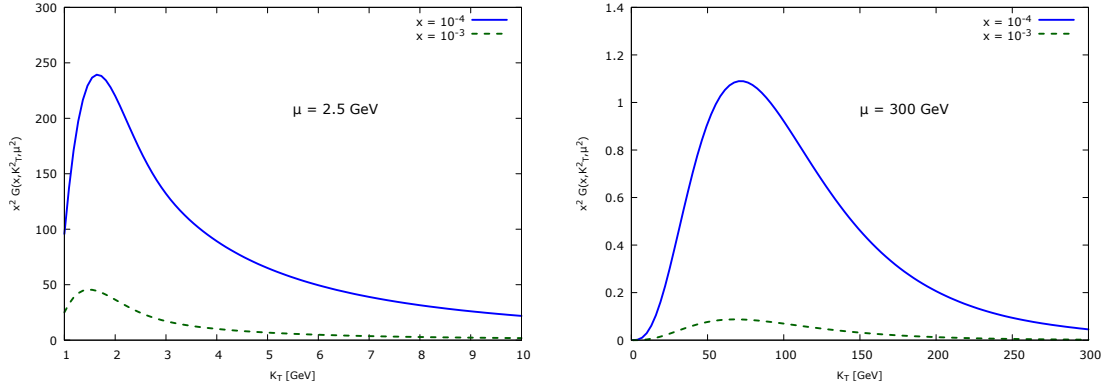
Figure 1: The density G entering the DDT formula for two different values of x and two fixed values of $\mu = P_T = 2.5\,\mathrm{GeV}$ (left) and $300\,\mathrm{GeV}$ (right). The PDF set used here was GRV98 [33].

leading-power theorem holding to all orders in α_s, it has been shown in [40] that it holds to next-to-logarithmic accuracy for the latter case.

Before discussing the power corrections to (2) let us make some general comments. The twist corrections to deep inelastic structure functions, i.e. the corrections $\mathcal{O}\left(1/Q^2\right)$ with Q^2 being the photon virtuality, were studied long time ago in the context of the operator product expansion (OPE) [41] and using Feynman diagrams [42]. While OPE is very general, it becomes very complicated for more exclusive processes (see e.g. [43] and [44]). As for jet production in hadron-hadron collisions no higher twist factorization exists (see also a discussion of power corrections coming from heavy quarks in the end of this subsection). On the other hand there are approaches which take into account all power corrections of a certain class. At very large energies the logs of the form $\log\left(1/x\right)$, where x is a fraction a hadron longitudinal momentum carried by the parton, become large and can be resummed by means of the BFKL equation. Let us note, however, that it is often arguable if such logs should be resummed at currently achievable energies, as most of the observables measured at LHC can be explained using collinear factorization supplemented by the DGLAP-type parton showers. Nevertheless, the BFKL formulation leads to HEF, which as mentioned in the Introduction resums the power corrections of the form K_T/μ. We shall describe HEF in more details in Subsection 2.3.

For completeness let us discuss a special case when $K_T \gg \mu$. For the case of the Drell-Yan process this kinematic region was studied in [45, 46], before the DDT formula was established. The corrections of this type can be obtained calculating explicitly additional emission by means of $2 \to 3$ process, away from the singular (soft and/or collinear) region. In particular, the HEF partially recovers this perturbative limit for certain UGDs.

Finally, let us make some comments on the power corrections coming from the heavy quark masses. Actually, they can be explicitly taken into account in the hard cross section, order-by-order. The problem is however, that by doing so the cross section becomes infra-red unsafe for large p_T, i.e. we shall encounter logs of the type $\log\left(P_T^2/m_Q^2\right)$ where m_Q is the mass of a heavy quark Q. This problem can typically be addressed by so-called general-mass scheme, which supplements the hard cross section with a proper subtraction terms (see [47] for a general proof and [48] for a formulation for jets in DIS at NLO). However, for jets in hadron-hadron collisions

there is a problem with the cancellation of soft singularities when incoming lines are massive [49] and thus the power corrections are unlikely to be controlled using the general-mass schemes. We shall ignore all these complications as we will be focused on pure gluonic contributions, which should dominate at high energies.

2.2   Singularity $p_T \to 0$ and soft cutoff

In this section we shall discuss in detail the concept of the soft transverse momentum cutoff. We shall restrict our considerations to gluons only. This is done for two major reasons. First, the gluons dominate at high energies and this is sufficient to illustrate all the effects we analyze in the paper (we do not aim at giving any predictions or comparisons with data). Second, later on we shall make comparisons across models including HEF, which is basically restricted only to gluons dominating at high energies. In principle one could consider off-shell quarks, but the subject is still poorly developed and would unnecessarily complicate our study (see [50, 51] for selected recent results).

Let us start by writing LO contribution to (1). We parametrize the momenta of hadrons as

$$p_A^\mu = \sqrt{\frac{S}{2}}\, n_+^\mu, \quad p_B^\mu = \sqrt{\frac{S}{2}}\, n_-^\mu\,, \tag{5}$$

where $n_\pm = (1, 0, 0, \pm 1)$ and $S = 2 p_A \cdot p_B$ is the CM energy squared. The kinematics of the hard subprocess $g\,(k_A)\,g\,(k_B) \to g\,(p_1)\,g\,(p_2)$ is

$$k_A^\mu = x_A p_A^\mu, \quad k_B^\mu = x_B p_B^\mu\,, \tag{6}$$

$$p_1^\mu = z_1 p_A^\mu + \frac{-p_{T1}^2}{z_1 S}\, p_B^\mu + p_{T1}^\mu, \quad p_2^\mu = z_2 p_A^\mu + \frac{-p_{T2}^2}{z_2 S}\, p_B^\mu + p_{T2}^\mu\,, \tag{7}$$

with momentum conservation $k_A + k_B = p_1 + p_2$. Obviously z_1, z_2 are directly related to rapidities $y_{1,2}$ in the following way

$$z_{1,2} = \frac{|\vec{p}_{T\,1,2}|}{\sqrt{S}}\, e^{\,y_{1,2}}\,, \tag{8}$$

with $p_{T1,2}^2 = -|\vec{p}_{T1,2}|^2$. Due to the transverse momentum conservation both outgoing jets have exactly the same transverse momentum $|\vec{p}_{T1}| = |\vec{p}_{T2}|$. In what follows we shall simply use notation $|\vec{p}_{T1,2}| \equiv p_T$ for brevity. In the above kinematics, the cross section can be calculated as

$$\sigma_{2\text{jet}} = \frac{1}{16\pi} \int \frac{dp_T^2}{p_T^4} \int \frac{z_1 dz_1\, z_2 dz_2}{(z_1 + z_2)^4}$$
$$f_{g/H}\left(z_1 + z_2, \mu^2\right) f_{g/H}\left(\frac{p_T^2}{S}\, \frac{z_1 + z_2}{z_1 z_2}, \mu^2\right) \frac{1}{2}\, |\overline{\mathcal{M}}|^2_{gg \to gg}\,(z_1, z_2)\,, \tag{9}$$

where the amplitude squared and averaged/summed over spin and color reads

$$|\overline{\mathcal{M}}|^2_{gg \to gg}\,(z_1, z_2) = g^4\, \frac{9}{2}\, \frac{\left(z_1^2 + z_1 z_2 + z_2^2\right)^3}{z_1^2 z_2^2\,(z_1 + z_2)^2}\,. \tag{10}$$

7

Typically, as the hard scale μ one chooses the p_T of the jets. From (9) we see that the cross section diverges like

$$\frac{d\sigma_{2\text{jet}}}{dp_T^2} \sim \frac{\alpha_s^2\left(p_T^2\right)}{p_T^4}\,.\tag{11}$$

In the pioneering work [5] the MPI model was constructed with $\sigma_{2\text{jet}}$ modified to remove this singularity by defining

$$\sigma'_{2\text{jet}} = \int \frac{d\sigma_{2\text{jet}}}{dp_T^2} \frac{p_T^4}{\left(p_T^2 + p_{T0}^2\left(S\right)\right)^2} \frac{\alpha_s^2\left(p_T^2 + p_{T0}^2\left(S\right)\right)}{\alpha_s^2\left(p_T^2\right)}\,,\tag{12}$$

where $p_{T0}\left(S\right)$ is the model parameter we have briefly discussed in the Introduction. For example in version 8.1 of pythia it is defined as

$$p_{T0}\left(S\right) = 2.28 \left(\frac{\sqrt{S}}{7\,\text{TeV}}\right)^{0.215}\,\text{GeV}\,.\tag{13}$$

for standard pythia settings (including pre-determined PDF sets to be used by default). Let us mention, that the MPI model and the entire event generation procedure in pythia is very complex, much more then the simple Eq. (12). Nevertheless Eq. (12) constitutes one of the core building blocks of this powerful program.

The p_T spectrum of minijets $d\sigma'_{2\text{jet}}/dp_T^2$ within the presented model should exhibit a strong suppression for small p_T, slowly growing with energy. It is interesting to ask if such a suppression could be directly observed. Putting this question aside, we will simply calculate (see Section 4) the inclusive dijet production in the small p_T region using pythia and compare with the minijet spectrum $d\sigma'_{2\text{jet}}/dp_T^2$. There are a few interesting features of this calculation (thought to be more realistic than (12)) which will be discussed later.

2.3   High Energy Factorization

Let us now discuss how the power corrections in (2) can be taken into account in k_T-factorization (we use the terms 'high energy factorization' and 'k_T-factorization' interchangeably in the present work, although both terms have different origin).

In k_T-factorization the cross section is calculated as a convolution of so-called unintegrated gluon distributions (UGDs) and an off-shell matrix element. UGDs depend not only on longitudinal momentum fractions x, but also on the transverse momenta k_T of the gluons – a feature neglected in the collinear factorization due to the power counting. For the first time k_T-factorization was used in [11] for inclusive jet production at high energies using basically $2 \rightarrow 1$ process $g^*g^* \rightarrow g$. Let us note that the $2 \rightarrow 1$ process does not exist when the incoming partons are on-shell and collinear, but it appears at lowest order in the k_T factorization approach. Later, a similar idea (originally called HEF) was used to compute heavy quark production [12–15] by means of a gauge invariant matrix element for $g^*g^* \rightarrow Q\overline{Q}$ which was extracted from the Green function utilizing suitable eikonal projectors. The UGDs were assumed to undergo BFKL evolution. A natural step forward was to adopt the HEF to account for jet production processes at high energy. Thus, the HEF has been extended to all channels [52], including gluons. At small x the forward jets are especially interesting. They can be treated in a limiting case of HEF, where one of the gluons becomes on-shell [53–55]. In this approximation, this gluon is treated as a 'large-x' gluon and is assigned a standard collinear PDF. In the Color Glass Condensate (CGC) approach [56] a similar idea was used to study forward particle production in saturation
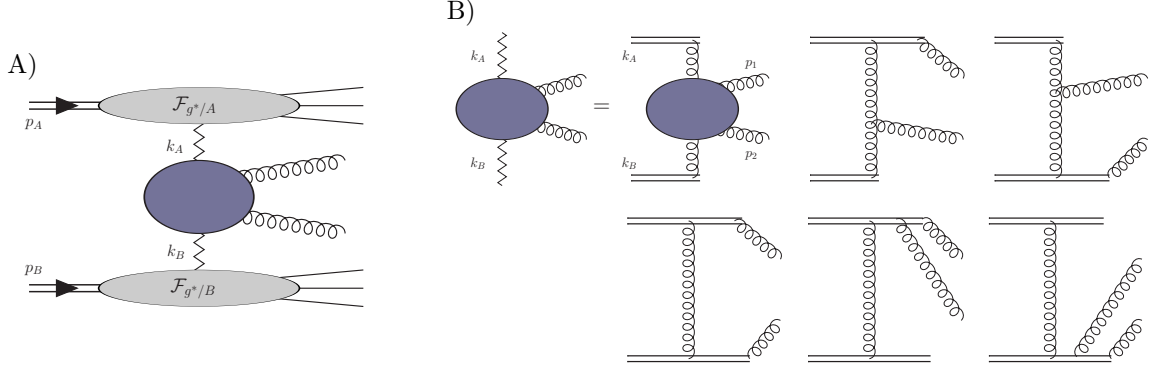
Figure 2: A) Schematic representation of the factorization formula (14) B) The hard gauge invariant tree level off-shell process expressed in terms of a matrix element of straight infinite Wilson lines, with the slopes being p_A (top) and p_B (bottom). The blue blob on the r.h.s. denotes a standard QCD contribution with four and triple gluon vertices. Only planar (color-ordered) diagrams are shown.

domain and exists under the name of the 'hybrid' formalism [57]. In fact, the hybrid version of HEF can be derived from CGC in the so called dilute limit (i.e. the case when the parton density of the target hadron is not large) [58, 59]. Several observables relevant for LHC have been calculated within the hybrid HEF, see Refs. [51, 60–63]. In the present work we are not concerned with forward jets thus we shall not use the hybrid version of HEF, but the original one with two off-shell incoming particles.

The factorization formula for HEF reads (including only gluons)

$$d\sigma_{AB \to gg} = \int d^2 k_{T\,A} \int \frac{dx_A}{x_A} \int d^2 k_{T\,B} \int \frac{dx_B}{x_B}$$
$$\mathcal{F}_{g^*/A}\left(x_A, k_{T\,A}; \mu\right) \mathcal{F}_{g^*/B}\left(x_B, k_{T\,B}; \mu\right) d\hat{\sigma}_{g^*g^* \to gg}\left(x_A, x_B, k_{T\,A}, k_{T\,B}; \mu\right), \quad (14)$$

where $\mathcal{F}_{g^*/A}$, $\mathcal{F}_{g^*/B}$ are UGDs for hadrons A, B and $d\hat{\sigma}_{g^*g^* \to gg}$ is the partonic cross section build up from the gauge invariant $g^*g^* \to gg$ amplitude (Fig. 2A). The momenta of the off-shell gluons have the following form relevant to the high energy approximation:

$$k_A \simeq x_A p_A + k_{TA}, \quad k_B \simeq x_B p_B + k_{TB}. \quad (15)$$

The off-shell partonic cross section is defined by a reduction of the Green's function, where the off-shell legs k_A and k_B are contracted with eikonal projectors proportional to p_A^μ and p_B^μ. Unlike the $g^*g^* \to q\bar{q}$ amplitude used in original HEF, the gluonic off-shell hard process cannot be just calculated from the standard Feynman diagrams in a gauge invariant way. There are number of ways this can be done in consistency with the high energy approximation used to define the hard process. First, one can include the bremsstrahlung from the lines to which the hard process is attached. At high energies those lines are eikonal. Such idea was used in [52] to calculate $g^*g^* \to gg$ and later in [64] a general method for helicity amplitudes as well as numerical algorithm for any number of partons was developed. Second, in the approximation used to derive (14) the gauge invariant amplitude for $g^*g^* \to gg$ is equivalent to the Lipatov's vertex $RRPP$ [65, 66] in the quasi-multi-regge kinematics. A more general approach is to consider matrix element of straight infinite Wilson line operators with the polarization of the

9

off-shell gluon identified as the Wilson line slope [67]. This method can be also used beyond the high energy approximation [68, 69]. Finally, a method generalizing the BCFW recursion [70, 71] to the off-shell case is also available [72, 73]. Although the Lagrangian method of [65] is the most general, in practical computations, especially for multiple external legs, the other mentioned methods are more efficient. For the hybrid version of (14) a very efficient method of calculating helicity amplitudes for $g^*g \to g \ldots g$ was found in [74]. Some other applications and different ways of calculating $g^*g^* \to gg$ were given e.g. in [52, 75]. Moreover, many other studies have been done using k_T-factorization, see for example [51, 76–81].

The partonic cross section in (14) is defined as

$$d\hat{\sigma}_{g^*g^* \to gg} = \frac{1}{2x_A x_B S} \frac{1}{2} \left.\left|\overline{\mathcal{M}}\right|^2\right|_{g^*g^* \to gg} d\mathrm{PS} \,, \tag{16}$$

where $d\mathrm{PS}$ is the two-particle phase space while $\left.\left|\overline{\mathcal{M}}\right|^2\right|_{g^*g^* \to gg}$ is the amplitude squared for the gauge invariant off-shell process discussed above. Using the method of [67] it can be calculated as follows. First, the amplitude is decomposed into the color-ordered amplitudes [82]. For the one particular ordering of the external lines the color-ordered amplitude is given by the planar diagrams displayed in Fig. 2B in Feynman gauge. The double lines on the top and the bottom correspond to the Wilson line propagators. Calculation of these diagrams (with proper normalization) gives the following result for the square of the amplitude

$$|\mathcal{A}|^2 (k_A, p_1, p_2, k_B) = -\frac{g^4}{s^2 t^2 \bar{t}_1 \bar{t}_2} \frac{1}{k_{TA}^2 k_{TB}^2}$$

$$\left\{ k_{TA}^2 t\bar{t}_2 \left[k_{TA}^2 \left(k_{TB}^2 s\bar{s} + t\bar{t}_1 \bar{u}_1^2 \right) + 2\bar{t}_1 \bar{u}_1 W \right] + k_{TB}^2 t\bar{t}_1 \left[k_{TB}^2 \left(k_{TA}^2 s\bar{s} + t\bar{t}_2 \bar{u}_2^2 \right) + 2\bar{t}_2 \bar{u}_2 W \right] \right.$$

$$\left. + k_{TA}^2 k_{TB}^2 t \left[t \left(s^2 \bar{s}^2 + 2\bar{t}_1 \bar{t}_2 \bar{u}_1 \bar{u}_2 \right) + s\bar{s} \left(\bar{s}^2 t - 4\bar{t}_1 \bar{t}_2 \left(\bar{s} + \bar{t}_1 + \bar{t}_2 - t \right) \right) \right] + \bar{t}_1 \bar{t}_2 W^2 \right\}, \tag{17}$$

where

$$W = \left[s \left(\bar{s} t + \bar{t}_1 \bar{t}_2 \right) - \bar{s} t \left(\bar{s} + \bar{t}_1 + \bar{t}_2 - t \right) \right] \,. \tag{18}$$

Above we have used abbreviations $k_{TA,B}^2 \equiv \left| \vec{k}_{TA,B} \right|^2$. The standard and auxiliary Mandelstam invariants read

$$s = (k_A + k_B)^2 \,, \ t = (k_A - p_1)^2 \,, \ u = (k_A - p_2)^2 \,, \tag{19}$$

$$\bar{s} = (x_A p_A + x_B p_B)^2 \,, \ \bar{t}_{1,2} = (x_A p_A - p_{1,2})^2 \,, \ \bar{u}_{1,2} = (x_B p_B - p_{1,2})^2 \,. \tag{20}$$

They satisfy $s + t + u = -k_A^2 - k_B^2$ and $\bar{s} + \bar{t}_{1,2} + \bar{u}_{1,2} = 0$. The order of arguments in (17) corresponds to the order of the external legs (see Fig. 2B). The color dressed amplitude is obtained by summing over all noncyclic permutations of the external legs (minus equivalent permutations due to the relations like $|\mathcal{A}|^2 (k_A, p_1, p_2, k_B) = |\mathcal{A}|^2 (k_B, p_2, p_1, k_A)$, etc.)

$$\left.\left|\overline{\mathcal{M}}\right|^2\right|_{g^*g^* \to gg} = \frac{1}{(2\pi)^2} \frac{N_c^2}{(N_c^2 - 1)}$$

$$2 \left[|\mathcal{A}|^2 (k_A, p_1, p_2, k_B) + |\mathcal{A}|^2 (k_A, p_2, p_1, k_B) + |\mathcal{A}|^2 (k_A, p_1, k_B, p_2) \right] \,. \tag{21}$$

The factor $1/(2\pi)^2$ constitutes the helicity average for the off-shell gluons as their 'polarization' vectors can be thought of to be 'continuous'. It is because one can show that these polarizations are k_{TA}^μ / k_{TA} and k_{TB}^μ / k_{TB} which depend on the transverse angle spanning between 0 and 2π.

Using the same kinematics as for the collinear case (but now with (15) for initial states) we can write the cross section as

$$d\sigma_{AB \to gg} = \frac{1}{32\pi^2} \int d^2\vec{k}_{TA} d^2\vec{k}_{TB} \int \frac{dp_T^2 d\phi}{\left[z_1 \left(\vec{p}_T - \vec{K}_T \right)^2 + z_2 p_T^2 \right]^2} \int \frac{z_1 dz_1 \, z_2 dz_2}{(z_1 + z_2)^2}$$

$$\mathcal{F}_{g^*/A} \left(z_1 + z_2, k_{TA}, \mu \right) \mathcal{F}_{g^*/B} \left(\frac{1}{z_2 S} \left(\vec{p}_T - \vec{K}_T \right)^2 + \frac{1}{z_1 S} p_T^2, k_{TB}, \mu \right)$$

$$\frac{1}{2} \left| \overline{\mathcal{M}} \right|^2_{g^* g^* \to gg} \left(z_1, z_2, \vec{k}_{TA}, \vec{k}_{TB}; \mu \right) , \quad (22)$$

where

$$\vec{K}_T = \vec{k}_{TA} + \vec{k}_{TB} . \quad (23)$$

The invariants in (17) can be easily expressed in terms of integration variables in (22). Comparing this with the collinear expression (9) we see that the singularity $p_T^2 \to 0$ can be potentially regularized by a nonzero K_T. Let us note, however, that K_T can be zero even if k_{TA}, k_{TB} generated in UGDs are nonzero. In fact due to the transverse momentum conservation whenever the jets are back-to-back $K_T = 0$ and the singularity $p_T^2 \to 0$ remains bare. For nonzero k_{TA}, k_{TB} the K_T depends on relative orientation of the vectors $\vec{k}_{TA}$, $\vec{k}_{TB}$. Since UGDs do not generally depend on angles, the only correlations can be hidden inside the matrix element. Moreover, the expression (22) has to be integrated over transverse variables to be actually compared with the collinear expression. We shall later perform a detailed numerical study and see whether the modification of $1/p_T^4$ factor due to K_T can produce a cutoff similar to minijet models. This in principle would be possible, as one can check that the median of the transverse momenta given by UGDs grows with decrease of x. Anticipating the result, however, let us recall, that actually (22) should be used in the hard scattering regime, that is for $\mu \sim p_T$ large. This can be also understood by realizing that the main contribution to $\left| \overline{\mathcal{M}} \right|^2_{g^* g^* \to gg}$ comes from the collinear region. In fact it can be shown that

$$\int_0^{2\pi} \frac{d\alpha_1}{2\pi} \frac{d\alpha_2}{2\pi} \left| \overline{\mathcal{M}} \right|^2_{g^* g^* \to gg} \left(z_1, z_2, \vec{k}_{TA}, \vec{k}_{TB}; \mu \right) = \left| \overline{\mathcal{M}} \right|^2_{gg \to gg} \left(z_1, z_2; \mu \right)$$

$$+ \mathcal{O} \left(\frac{k_{TA}}{\mu} \right) + \mathcal{O} \left(\frac{k_{TB}}{\mu} \right) + \mathcal{O} \left(\frac{k_{TA} k_{TB}}{\mu^2} \right) , \quad (24)$$

where α_1, α_2 are the angles on the transverse plane of the vectors $\vec{k}_{TA}$, $\vec{k}_{TB}$ and the first term on the r.h.s. is the collinear matrix element. By using the above expression and expanding in powers of k_T/μ one can find systematically power expansion of the cross section. The UGDs are typically peaked for small values of k_{TA}, k_{TB} thus the collinear contribution is the dominant one (the leading power contribution). Therefore one should expect that the applicability of (22) is in the high p_T domain.

Let us make now a few comments about the HEF. The first comment concerns the collinear limit of (22). One would expect that for large p_T the cross section $d\sigma/dp_T$ calculated converges to the collinear one (9). Performing the expansion (24) and retaining the first collinear contribution only we are left with integrals in (22) of the type

$$\int^{k_{T\max}^2} dk_{TA}^2 \, \mathcal{F}_{g^*/A} \left(x_A, k_{TA}, \mu \right) \equiv f_{g/A}^{(k_{T\max})} \left(x_A, \mu \right) , \quad (25)$$

where $k_{T\max}$ is the upper bound on k_T which in practice is constrained by the grid size of the UGDs or specific kinematic cuts. The point is that the function $f_{g/A}^{(k_{T\max})}$ is in general not exactly a collinear gluon PDF, which is defined as

$$f_{g/A}\left(x_A, \mu\right) = f_{g/A}^{(\mu)}\left(x_A, \mu\right) . \tag{26}$$

Thus, we will overshoot the collinear result if the hard scale μ is not too large and the UGDs do not fall very rapidly with k_T. In other words, the convergence to the collinear result for finite μ is rather weak. The remedy could be to set $k_{T\max} = \mu$, but this not inherent part of the HEF. Let us illustrate the above with a concrete and practical example. According to the Kimber-Martin-Ryskin (KMR) prescription [19, 20] (actually its commonly used simplified form), an UGD can be constructed from a collinear PDF as follows:

$$\mathcal{F}_{g^*/H}\left(x, k_T, \mu\right) = \frac{\partial}{\partial k_T^2} \left[f_{g/H}\left(x, k_T\right) T_g\left(k_T, \mu\right) \right] , \tag{27}$$

where T_g is the Sudakov form factor. We see that the $k_{T\max}$ has to be equal to μ in order to recover $f_{g/H}$ upon integration over k_T.

In order to address another possible issue of HEF, let us consider the cross section as a function of the jet disbalance K_T, $d\sigma/dK_T$. It can be calculated within HEF using (22). Let us now find the collinear limit of $d\sigma/dK_T$. It is easy to see, that it will not converge to the DDT formula (2). This is not necessarily a problem, as the natural domains of applicability of HEF formula and DDT are very different. Nevertheless, it would be interesting to have a formula which includes subleading powers of K_T while possessing the leading twist limit given by (2). We shall construct such a formula in the next subsection.

Finally, let us mention that in practical applications it is convenient to use Monte Carlo programs to generate various observables for jets, instead of using the formulae like e.g. (22). Thus in our study we use an implementation of HEF in a computer program [83] which relies on the foam adaptive Monte Carlo [84]. It allows to generate partonic events ('weighted' or 'unweighted'), store them and make further analysis in a convenient way. No parton shower or hadronization is done in the current version. Let us however mention that the k_T dependence of gluon distributions acts much like the initial state parton shower (see e.g. [61, 85]).

2.4 Extension of DDT beyond leading power

In order to make our analysis as complete as possible, we will construct now a version of HEF which in the leading power limit reduces to the DDT formula (2) for the dijet disbalance spectrum. The goal of doing this is to use broad spectrum of models with internal gluon k_T. In HEF described in the previous subsection the k_T dependent UGDs take into account two ladders of initial state emissions for each colliding hadron; it is most transparent when UGDs are considered within the KMR approach (27) (see Fig. 2A). There are no final state emission ladders in HEF, whilst the DDT formula (2) has a one ladder attached to each leg of the hard process, including the final state lines (Fig. 2B) [31]. Of course, the DDT formula is the leading twist expression, on the contrary to HEF. Below, we shall construct a HEF-based model which has a similar philosophy to the DDT, but includes power corrections.
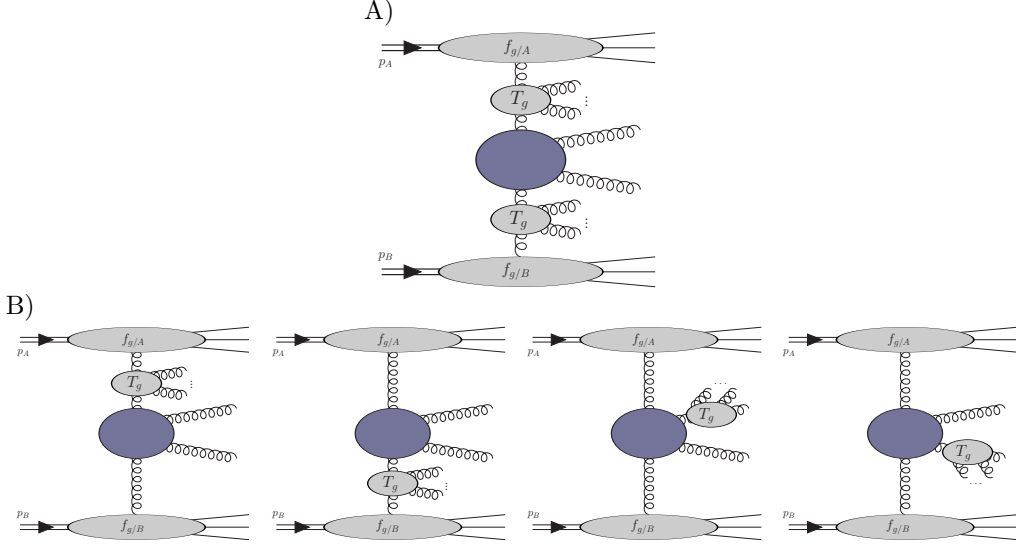
Figure 3: A) In HEF with the KMR prescription (27) the k_T of initial state gluons on both sides is produced by the gluon PDF and the Sudakov form factor B) In the leading twist DDT formula of Eq. (2) one ladder of emissions is associated with each leg of the hard process.

Let us first write (2) as

$$
\frac{d\sigma_{2\text{jet}}}{dK_T^2} = 2 \int \frac{dx_A}{x_A} \frac{dx_B}{x_B} \, d\hat{\sigma}_{gg \to gg} \left(x_A, x_B; \mu^2 \right)
$$

$$
\times \left\{ \frac{\partial}{\partial K_T^2} \left[f_{g/A} \left(x_A; K_T^2 \right) T_g \left(K_T^2, \mu^2 \right) \right] f_{g/B} \left(x_B; K_T^2 \right) T_g^3 \left(K_T^2, \mu^2 \right) \right.
$$

$$
\left. + f_{g/A} \left(x_A; K_T^2 \right) f_{g/B} \left(x_B; K_T^2 \right) T_g^3 \left(K_T^2, \mu^2 \right) \frac{\partial}{\partial K_T^2} T_g \left(K_T^2, \mu^2 \right) \right\}, \quad (28)
$$

where we have used the symmetry with respect to exchange of hadrons $A \leftrightarrow B$ (this gives a factor of 2). Building upon the above formula and using (27) we now define

$$
\frac{d\sigma_{2\text{jet}}^{(\text{IDDT})}}{dK_T^2} = \frac{d\sigma_{2\text{jet}}^{(\text{IS})}}{dK_T^2} + \frac{d\sigma_{2\text{jet}}^{(\text{FS})}}{dK_T^2}, \quad (29)
$$

where the 'initial state' contribution is

$$
d\sigma_{2\text{jet}}^{(\text{IS})} = 2 \int \frac{dx_A}{x_A} \frac{dx_B}{x_B} \int d^2 K_T \, d\hat{\sigma}_{g^* g \to gg} \left(x_A, x_B, \vec{K}_T; \mu^2 \right)
$$

$$
\mathcal{F}_{g^*/A} \left(x_A, K_T, \mu \right) f_{g/B} \left(x_B, K_T^2 \right) T_g^3 \left(K_T^2, \mu^2 \right), \quad (30)
$$

while the 'final state' contribution is

$$
d\sigma_{2\text{jet}}^{(\text{FS})} = 2 \int \frac{dx_A}{x_A} \frac{dx_B}{x_B} \int d^2 K_T \, d\hat{\sigma}_{gg \to gg^*} \left(x_A, x_B, \vec{K}_T; \mu^2 \right)
$$

$$
\times f_{g/A} \left(x_A; K_T^2 \right) f_{g/B} \left(x_B; K_T^2 \right) T_g^3 \left(K_T^2, \mu^2 \right) \mathcal{T}_g \left(K_T^2, \mu^2 \right). \quad (31)
$$

13

We have defined the final state transverse momentum distribution as

$$\mathcal{T}_g\left(K_T^2, \mu^2\right) = \frac{\partial}{\partial K_T^2} T_g\left(K_T^2, \mu^2\right).$$ (32)

The Sudakov form factor we use is given by the following formula [31]:

$$T_g\left(k_T^2, \mu^2\right) = \exp\left\{-\int_{k_T^2}^{\mu^2} \frac{dp_T^2}{p_T^2} \int_\Delta^1 dz \frac{\alpha_s\left(p_T^2\right)}{2\pi} \left[(1-z)P_{gg}(z, \Delta) + N_f P_{qg}(z)\right]\right\},$$ (33)

where

$$P_{gg}(z, \Delta) = 2C_A\left(\frac{z}{1 - z + \Delta} + \frac{1 - z}{z} + z(1-z)\right),$$ (34)

$$P_{qg}(z) = \frac{1}{2}\left(z^2 + (1-z)^2\right).$$ (35)

The cutoff parameter Δ is taken to be $\Delta = k_T^2/\mu^2$. We note that there are various forms of the cutoff parameter in the literature, see for example [19]. The partonic cross section $d\hat{\sigma}_{g^*g\to gg}$ is calculated in the exact same way as in the hybrid HEF described before, taking into account the gauge invariant off-shell amplitude with only one leg being off-shell

$$d\hat{\sigma}_{g^*g\to gg} = \frac{1}{2x_A x_B S} \frac{1}{2} \left|\overline{\mathcal{M}}\right|^2_{g^*g\to gg} d\text{PS},$$ (36)

where $\left|\overline{\mathcal{M}}\right|^2_{g^*g\to gg}$ was calculated for instance in [53] and using helicity amplitudes in [74]. It reads

$$\left|\overline{\mathcal{M}}\right|^2_{g^*g\to gg} = \frac{g^4}{2\pi} \frac{N_c^2}{N_c^2 - 1} \frac{\left(\bar{s}^4 + \bar{t}_1^4 + \bar{u}_1^4\right)\left(s\bar{s} + t\bar{t}_1 + u\bar{u}_1\right)}{s\bar{s}t\bar{t}_1 u\bar{u}_1},$$ (37)

with the invariants defined in (19),(20), but now $k_{TA} \equiv K_T$. In the above form the on-shell limit is visible right away: when $K_T \to 0$ we have $\bar{s} \to s$, $\bar{t}_1 \to t$, $\bar{u}_1 \to u$ and we get the known collinear result.

The partonic cross section with final state off-shell $d\hat{\sigma}_{gg\to gg^*}$ is a new construction and to our knowledge does not exist in the literature. It is constructed from the gauge invariant off-shell amplitude with the final state particle taken off-shell

$$d\hat{\sigma}_{gg\to gg^*} = \frac{1}{2x_A x_B S} \frac{1}{2} \left|\overline{\mathcal{M}}\right|^2_{gg\to gg^*} d\text{PS}\left(K_T^2\right),$$ (38)

where $d\text{PS}\left(K_T^2\right)$ is the two-particle phase space to produce a spacelike state with mass K_T^2. Let us now explain, how the amplitude $\left|\overline{\mathcal{M}}\right|^2_{gg\to gg^*}$ is calculated, as it differs from the standard way the HEF amplitudes are obtained.

First consider the kinematics involved in (31), see Fig. 4A. The idea is that first the two states are produced: an on-shell gluon p_2 and the off-shell one with momentum $\tilde{p}_1$, $\tilde{p}_1^2 = -K_T^2$. Next, this off-shell dressed gluon undergoes emissions described by $\mathcal{T}_g$ defined in (32) and becomes on-shell $p_1 = \tilde{p}_1 + K_T$, $p_1^2 = 0$. The first stage happens via the off-shell gauge invariant process $g\left(k_A\right)g\left(k_B\right) \to g^*\left(\tilde{p}_1\right)g\left(p_2\right)$ calculated from diagrams depicted in Fig. 4B according to the prescription of [67]. As the Wilson line slope we take here the momentum p_1 (not the eikonal vectors $p_{A,B}$, as it was the case for HEF), so that

$$\tilde{p}_1 \cdot p_1 = 0, \quad K_T \cdot p_1 = 0.$$ (39)
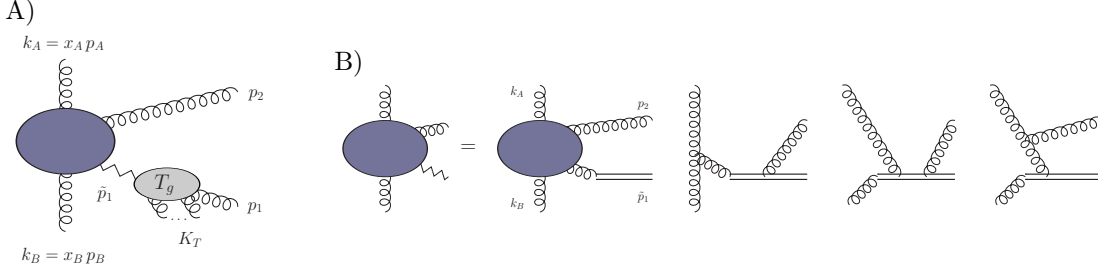
14

A)

B)

Figure 4: A) Momentum assignment in the final state contribution to (29); the final state momentum $\tilde{p}_1$ is off-shell. B) Diagrams contributing to the gauge invariant final state off-shell process; the Wilson line slope is given by the vector p_1 so that $\tilde{p}_1 \cdot p_1 = 0$.

The result reads

$$\left|\overline{\mathcal{M}}\right|^2_{gg \to gg^*} = \frac{g^4}{2} \frac{N_c^2}{N_c^2 - 1} \frac{\left(\tilde{s}^4 + \tilde{t}^4 + \tilde{u}^4\right)\left(s\tilde{s} + t\tilde{t} + u\tilde{u}\right)}{s\tilde{s}t\tilde{t}u\tilde{u}} . \tag{40}$$

It looks basically the same as (37) but now

$$\tilde{s} = (p_2 + p_1)^2, \quad \tilde{t} = (x_A p_A - p_1)^2, \quad \tilde{u} = (x_B p_B - p_1)^2, \tag{41}$$

$$s = (p_2 + \tilde{p}_1)^2, \quad t = (x_A p_A - \tilde{p}_1)^2, \quad u = (x_B p_B - \tilde{p}_1)^2. \tag{42}$$

The above final state contribution differs from the standard approach adapted in the event generators. In the latter, the on-shell $gg \to gg$ process is augmented with the final state splitting $g \to gg$ with probability related to the Sudakov form factor. Formally, the splitting is purely collinear, as the transverse momenta are integrated over. This part of the generation is purely perturbative based on the time-like DGLAP evolution. Then, the true exclusive kinematics has to be reconstructed/modelled. In the case of the present model, the final state line is space-like, with explicit (non-integrated) off-shellnes. Note, that since this final state does not split into on-shell partons the fact it is space-like is perfectly valid.

It is important to mention that, by construction, the maximal allowed value of K_T is $K_{T\max} = \mu$. It is easy to see that then, in the leading power approximation we recover both the collinear result (1) and the DDT formula (2). In what follows we shall abbreviate the new model as IDDT (an 'improved DDT').

We have implemented the IDDT approach in a computer program [83] and in Fig. 5 we show the results of the consistency checks we have performed (for a detailed description of the setup and cuts see the next section). First, we compare the leading power limit of the IDDT with the collinear result for the p_T spectrum. We see (Fig. 5A) that they match ideally. We also show separately the contributions from the 'initial state' (30) and 'final state' cross sections. Next, we compare the spectrum in the jet disbalance K_T with the one obtained from the DDT formula (Fig. 5B) and find a perfect agreement. Thus we have gained exactly the properties we wanted, that is the formula (29) has the collinear and the DDT limits at leading power.

In the end, let us stress that the above construction is a model of higher twists, not a strict QCD derivation. We have neglected all the details concerning factorization and higher order corrections. Our aim was to catch certain properties such a formula should have in order to study their effect on minijets.
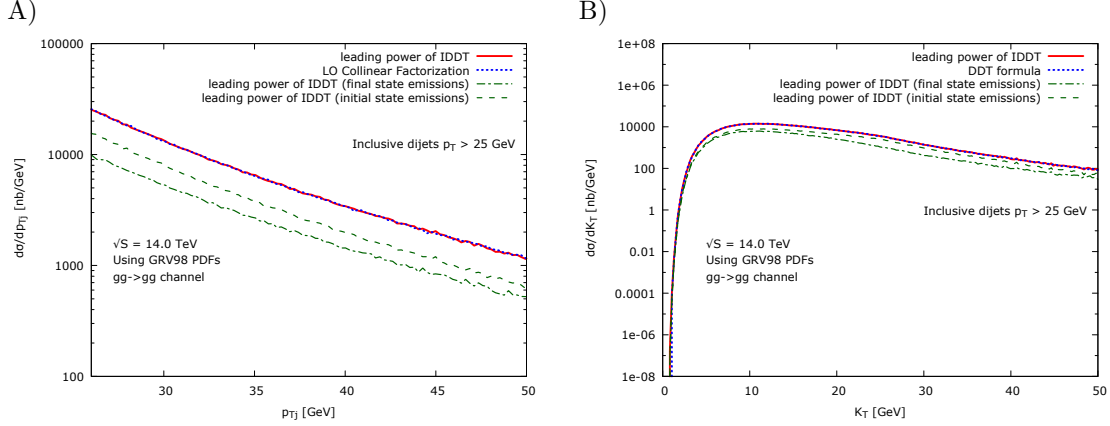
A)   B)

Figure 5: A) The leading power limit of the IDDT formula (29) for jet p_T spectrum in comparison with the LO collinear factorization. We see that it has the correct collinear limit as the solid line (IDDT) is on the top of the dotted line (collinear). We show also final state and initial state contributions of IDDT. B) The same but for the spectrum of jet disbalance and in comparison with the DDT formula.

3   Setup for numerical studies

Before presenting the detailed numerical results of the different minijet formulations, we shall first define the observable we are going to calculate as well as the kinematic cuts and details of the setups of the Monte Carlo programs.

The LO collinear jet formula (1) or (12) describes the production of exactly two jets. In more realistic simulations we deal with multi-parton configurations and a more careful definition of two-jet cross section is needed. This concerns simulations using both pythia and Monte Carlo implementation of HEF or IDDT. In the following, we will consider inclusive dijet cross section with jets reconstructed using the anti-k_T algorithm with certain $p_{T\min}$ and $R = 0.5$ (if not stated otherwise). We require at least two jets to be above $p_{T\min}$. We tag the two hardest jets, but we do not order them in their p_T, thus the spectra for both jets are identical. We require both jets to fit within $[-4, 4]$ rapidity window.

We shall use three approaches: (i) pythia, (ii) HEF as described in Subsection 2.3, (iii) IDDT constructed in Subsection 2.4. For reference we sometimes use also the pure collinear formula (9). The approaches (i), (ii) and (iii) will be used in the direct study of minijets in Section 4, while the indirect minijet study shall utilize models (i) and (ii).

The pythia generator has two disjoint modules: 'soft QCD' and 'hard QCD'. The first one is used when all produced particles have transverse momenta around or slightly above p_{T0} cutoff. The second is suitable for high-p_T particles. From the point of view of minijet model, they differ by the fact that in the 'hard QCD' module the hardest binary collision does not have the suppression factor as in (12).

Whenever we use pythia we use some non-standard settings in order to make clean comparisons. First, we use only gluonic channel. Second, we use LO GRV98 [33] PDFs with matching LO α_s. The reason we use GRV98 instead of some more up-to-date sets in that we will compare pythia calculations to HEF with KMR in the low p_T region. This requires that the PDF used to construct KMR has to be defined for small enough scale, smaller than $1\,\text{GeV}$. As of today,

this requirement is satisfied only by GRV98 distribution.

Above are the generic settings. The other settings concerning MPIs or parton showers and hadronization will be determined when necessary. In the description of the plots we shall use the following abbreviations: PS for final state and initial state parton showers and HAD for hadronization. In order to comply with the minijet formula we choose the hard scale to be the average p_T of jets.

In our analysis within HEF we will use several UGDs: (i) the KMR gluon distribution [19, 20] given by (27) based on the GRV98 collinear PDF. Note, that this is actually a prescription of DDT; the genuine KMR prescription is much more complicated, but traditionally (27) functions as KMR in the literature. (ii) The Kwiecinski-Martin-Stasto (KMS) [86] gluon distribution which supplements the BFKL equation with the DGLAP corrections. More precisely it incorporates the kinematic constraint to maintain the energy conservation and the nonsingular parts of the gluon-gluon splitting function. This gluon distribution has been fitted to HERA F_2 data in [87] and we will call this set KMS-HERA. In [88] fits have been performed to the jet LHC data (using however only gluonic part of the KMS equation). We shall call this set KMS-LHC in what follows. (iii) The CCFM equation [27–29] taken from [89] and based on the computer code [90]. We note that various CCFM sets differ between each other and thus we are not making any conclusions regarding CCFM from our work. The important point of the CCFM equation is that it encodes both the BFKL and DGLAP limits through the angular ordering constraint. A very important difference between KMS and CCFM evolution equations is that KMS does not depend on the hard scale of the process. We shall see, that this feature is important for jet studies. Similar to CCFM, the KMR approach does encode the hard scale dependence through the Sudakov form factor. In fact, in certain limit the CCFM gluon distribution can be reduced to the one of KMR [91].

All numerical simulations for HEF are performed using the extension of the C++ program [83] briefly described in the end of Section 2.3.

4   Direct study of minijet suppression

In the present section we directly study p_T spectra of minijets, i.e. inclusive dijets with $p_T \gtrsim 2\,\text{GeV}$ using pythia and HEF/IDDT in the small p_T region. In particular, we will check whether the internal gluon k_T can give a jet suppression compliant with the minijet formula (12). We have already anticipated the result: the main contribution in HEF/IDDT at low p_T comes from the collinear region of small k_T which does not have the suppression factor built in. We shall check this through numerical analysis of the p_T spectra.

Before we explore the HEF, let us ask a question how the suppression of the minijet spectrum looks in a realistic model which implements it. To this end we use the 'soft QCD' module of pythia suitable for small p_T and calculate the inclusive dijet spectra as described in the Section 3. The result is presented in Fig. 6. First, we indeed see big suppression of the spectrum which means that every binary collision in the small p_T region is suppressed – this is the feature of the 'soft QCD' module of pythia; in the 'hard QCD' module the hardest binary collision is not suppressed (see also the discussion below). The suppression produced in pythia is much bigger then the one following from the naive $d\sigma'_{2\text{jet}}/dp_T$ spectrum of Eq. (12). This is because in the 'soft QCD' module of pythia the suppression is modelled by the Sudakov-like form factor, where (12) enters the Sudakov-like exponent. The suppression growing with the CM energy is clearly visible. Second, we observe an enhancement of the spectrum at moderate p_T as compared to the naive $d\sigma'_{2\text{jet}}/dp_T$ spectrum. This feature does survive the hadronization, as seen in the figure.
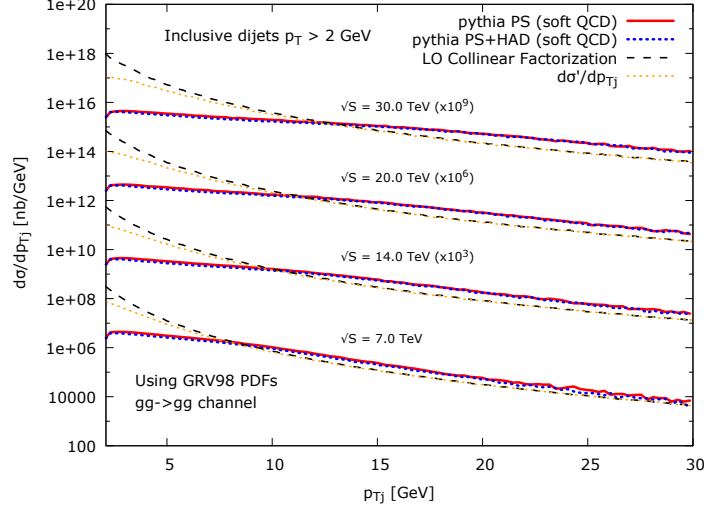
Figure 6: The suppression of minijet p_T spectrum comparing to the LO collinear factorization calculated with pythia using 'soft QCD' simulation with parton shower and with/without hadronization. The minijet model of Eq. (12) is also shown. The enhancement of the spectra with respect to the collinear factorization vanishes for sufficiently large p_Ts.

We shall come back to this enhancement later below and discuss it in more details.

Now we do the same for HEF and IDDT models. Here we are interested in a suppression with respect to the LO collinear factorization so we have to use the consistent gluon distributions. Thus we use the KMR based on GRV98 in HEF and we use the GRV98 itself in collinear factorization. We show the results in Fig. 7. First, we see that the direct suppression of the spectrum due to the internal gluon k_T is very small comparing to the minijet model (the top plot has the same horizontal scale as Fig. 6, while in the bottom plot we zoom the low-p_T region). Second, the suppression has the opposite energy dependence than (13), i.e. it becomes weaker when the energy is higher. This feature is present in both models HEF and IDDT and is qualitatively the same. Interestingly, the spectra for HEF (but not for IDDT) show an enhancement at moderate values of p_T relative to the collinear curves, similar to the one discussed above in pythia. This enhancement comes from the power corrections and vanishes for sufficiently high p_T. It is now interesting to compare this calculation to similar calculation made with pythia with the 'hard QCD' module with and without MPIs. Obviously, the 'hard QCD' cannot formally be used in the low-p_T region, but technically it can be done and this sheds some light on the interpretation of the results from Fig. 7. Namely, in the 'hard QCD' module the hard process does not have any p_T regularization factor and we expect the results to exhibit similar behavior to Fig. 7. We show these results in Fig. 8. By comparing them to Fig. 7 (in particular the bottom plots) we see that, qualitatively, the behaviour is very similar meaning that indeed the hard process in HEF (or IDDT) does not have the suppression of the kind (12). We also see that pythia with MPIs shows the same enhancement as HEF curves. This means that MPIs generate power corrections which are visible in the inclusive dijet spectra. We note that the enhancement vanishes for sufficiently large p_T as required by the AGK cutting rules [92].
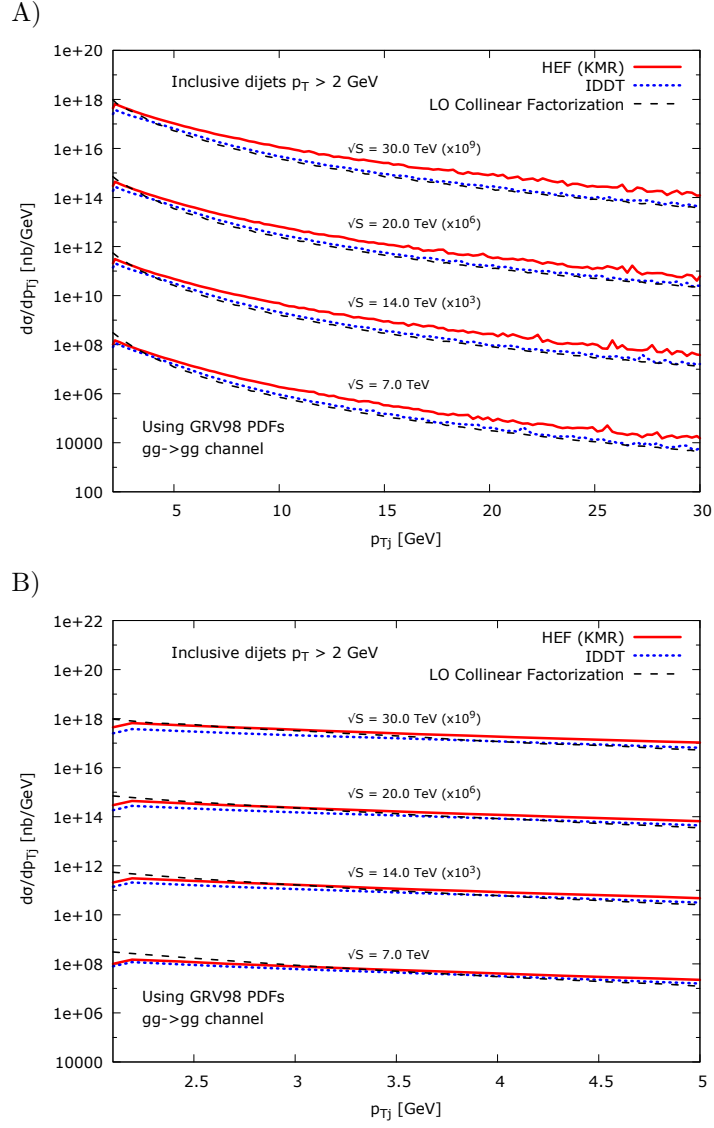
18

A)

B)

Figure 7: A) The same as in Fig. 6 but for HEF and IDDT approaches. B) The zoom into the low-p_T region of the top plot.
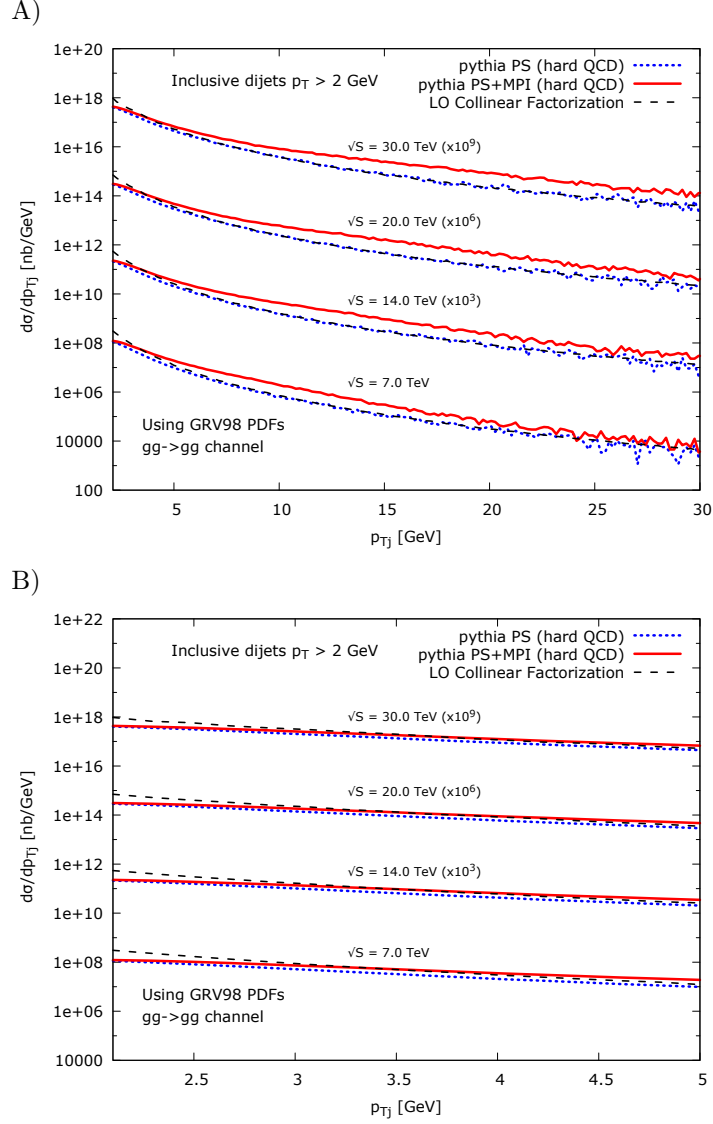
A)

B)

Figure 8: A) The same as in Fig. 6 but using pythia with 'hard QCD' module. It formally is not applicable for low-p_T but we use it on purpose to compare with HEF in this region (see the main text for details). B) The zoom into the low-p_T region of the top plot.

The similarity of the HEF spectra and pythia with 'hard QCD' module and MPI suggests that the power corrections in HEF may imitate MPIs in certain circumstances. The power corrections in HEF come from the tails in the transverse momentum of the UGDs. Actually, one can think of a collision within HEF as 'multiple collisions' weighted by a distribution of internal transverse momentum. This distribution is peaked at small transverse momentum, thus the collinear contribution (one of the multiple collision bundle) is dominant (the leading power contribution), and it is not suppressed. Further 'collisions' for larger internal transverse momenta are less important as the internal transverse momentum distribution falls off quickly. However, those sub-leading power corrections may exhibit different energy behavior. We shall investigate this point in the next section.

5 Indirect study of minijets

In the previous section we saw that the internal k_T flowing into the hard process as in HEF/IDDT approaches does not give the suppression of dijet production compliant with the minijet model (12). This is simply because the off-shell $2 \to 2$ hard process is dominated by the leading power contribution for which the effect of internal gluon k_T is small. Thus, the next question we ask is about the relation of power corrections created in minijet model with MPIs and power corrections rendered in HEF. We stress that we consider here inclusive *dijet* production at relatively small transverse momenta. The spectra for very large p_T would not be affected by MPIs.

In order to support the above statement that minijet model with MPI can generate similar corrections to HEF let us have again a look at the p_T spectra. We can see from Fig. 7 and Fig. 8 that within HEF and pythia with MPIs there is an enhancement for larger p_T's comparing to the collinear result. Both IDDT and pythia without MPIs do not have this feature. The reason for the IDDT model to be quickly convergent to the collinear result is because, by construction, we do not allow K_T to be bigger than the hard scale μ. On the contrary, in HEF K_T may be anything allowed by the jet kinematics. Thus we may draw a conclusion that both MPI corrections to the hard process in pythia and power corrections in HEF may have similar components. In this section we will study this point. Because IDDT does not allow for sizeable power corrections we will not consider it in this section anymore.

First we take a closer look at the direct comparison of Figs. 7-8 for certain CM energy, say $\sqrt{S} = 14$ TeV (Fig. 9A). We see, that for larger p_T's both pythia with MPIs and HEF start to exhibit indeed a similar enhancement comparing to the collinear result, but further in p_T the pythia spectrum converges to the collinear one while HEF converges much more slowly. We calculate also the spectra of the dijet momentum disbalance K_T (Fig. 9B). We see that the MPIs in pythia model produce higher tail of the K_T spectrum, which in addition is close to the one from HEF. These calculations are interesting, but as discussed before they are extrapolated beyond the natural domain of the applicability of the models used; both pythia with the 'hard QCD' module and HEF require rather high p_T to be present. Let us remind that we used pythia with the 'hard QCD' module in order to enforce the statement that HEF is dominated by the hard process which does not have the suppression.

Thus we make another set of calculations, now requiring $p_T > 25$ GeV to get rid of the range in p_T which normally would be strongly suppressed. This is the domain of applicability of both pythia 'hard QCD' and HEF. The results are presented in Fig. 9C-D. As for the p_T spectrum, the situation does not change comparing to the smaller p_T cut. For the disbalance K_T spectrum, we see that at first the HEF tail drops below pythia with MPI, but later it again rises toward the model with MPIs. The IDDT model has a similar (unphysical) low-K_T behavior as the genuine
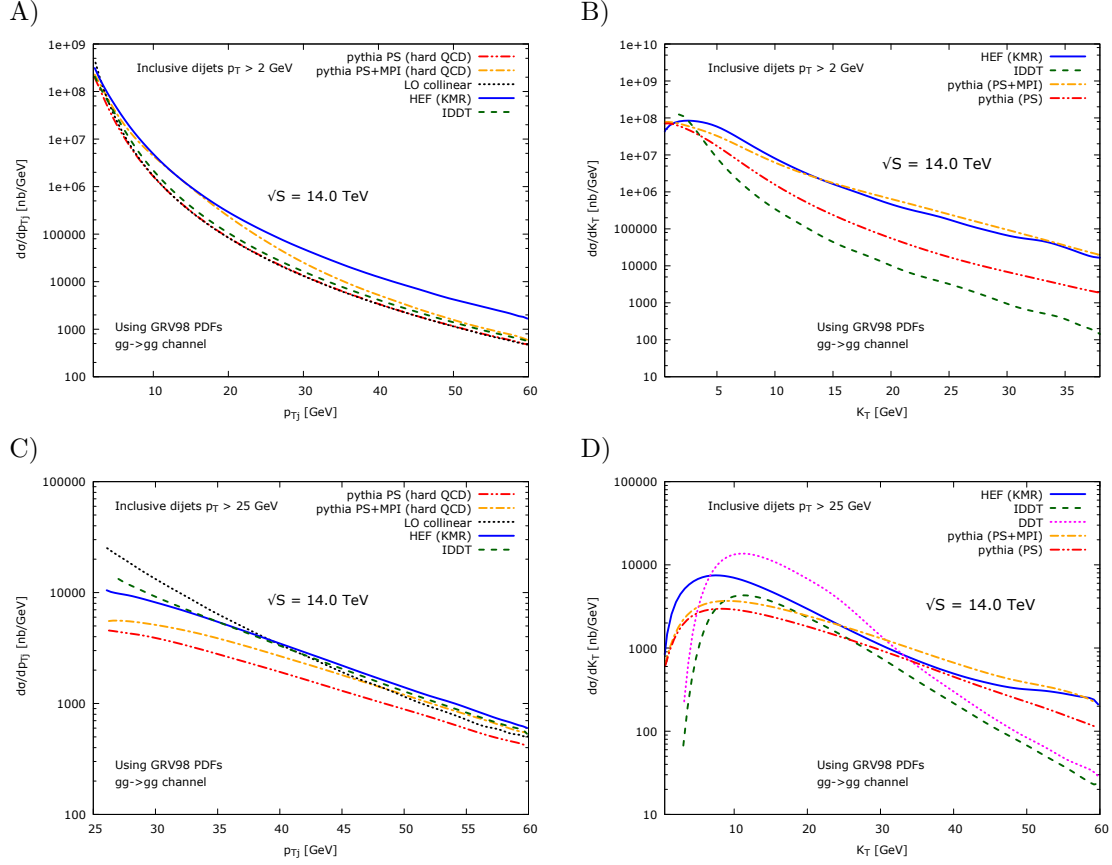
Figure 9: Comparison of the p_T spectra (left column) from various approaches and the spectrum of the dijet disbalance K_T (right column). The top row is for actual minijets, i.e. $p_T > 2\,\text{GeV}$ while the bottom row is for $p_T > 25\,\text{GeV}$.

DDT obtained from (2). It is important to stress, that in HEF we have been using the KMR based on GRV98 gluon distribution so far, and the features discussed above will be different for different UGDs. Similar, the shape of the pythia's enhancement will depend on the MPI model parameters, in particular on the p_{T0} parameter, as we will see below.

In order to better access the power corrections and study their energy dependence we propose the following observable. We investigate a differential cross section for inclusive dijets in the following variable:

$$\tau = \frac{K_T}{\mu} = \frac{2K_T}{p_{T1} + p_{T2}} \ . \tag{43}$$

It can be thought as being a measure of the 'twist content' in the approach. That is, the small $\tau \sim 0$ corresponds to the leading power, while $\tau > 1$ region is sensitive to higher power corrections. We expect that in HEF we will observe sizeable contribution to $\tau > 1$ region. On the other hand, in pythia generator the small momentum disbalance is generated by the parton shower, but it does not give significant contribution to $\tau > 1$. However, we expect that for $\tau > 1$ the contribution of MPIs should be visible, because almost uncorrelated partons originating in different hard collisions can produce very disbalanced jets. We shall come back to this later in this section.

We will be concerned with the shape of the τ distribution only. Since various UGDs often have different normalizations we shall divide the differential cross sections by the total cross section. We shall investigate this observable within the different approaches with a known minijet implementation for various p_{T0} settings (we mean pythia here) and HEF.

In Fig. 10 we show the results for the CM energy range $7 - 30$ TeV calculated in pythia for a few choices of the parameters in the parametrization of p_{T0} (S). Namely, we consider the following scenarios: (A) no MPI interactions, (B) constant $p_{T0} = 2.28$ GeV, (C) the standard implementation given by (13), (D) the choice (13) with the exponent taken to be around twice as big. In Fig. 11 we compare these scenarios for two fixed energies 14 TeV and 30 TeV. In a similar manner we calculate the spectra in τ using HEF in Fig. 12. We use the following UGDs described in Section 3: (A) KMR based on GRV98, (B) the CCFM, (C) the KMS-HERA and (D) the KMS-LHC.

Let us discuss first the spectra obtained from pythia. We see, that the distributions have a *bimodal* character, i.e. they have two peaks, one close to $\tau = 0$ and the second close to $\tau = 2$. The second peak (at large τ) is much weaker than the leading peak and its strength depends on the amount of MPIs present in the model: the more MPIs the stronger the second peak. This is seen when comparing the plots without suppression of minijets (Fig. 10B), throughout the increasing suppression (Figs. 10C-D), up to the 'infinite' suppression (i.e. no MPIs, Fig. 10A). This is even more visible from Fig. 11 where we compare these models for fixed energies. Let us note, that there is a peak close to $\tau = 2$ even if there are no MPIs. There are two types of events contributing to this region in that case. (i) Events due to the final state parton shower, where the emitted parton happens to be hard and emitted at an angle large enough to be reconstructed as a separate jet; this jet is then tagged together with the 'mother' jet. (ii) Events due to the initial state parton shower and accompanying beam remnant reconstruction. We have checked that the events involving initial state parton shower seem to happen more often than the final state splitting scenario. Naturally, these contributions depends on the jet algorithm. In case the MPIs are added, the second peak is enhanced relative to the first one, because now also (almost) uncorrelated partons may be clustered into jets that are tagged.

In order to investigate the energy dependence of the second peak we shall use the bimodality
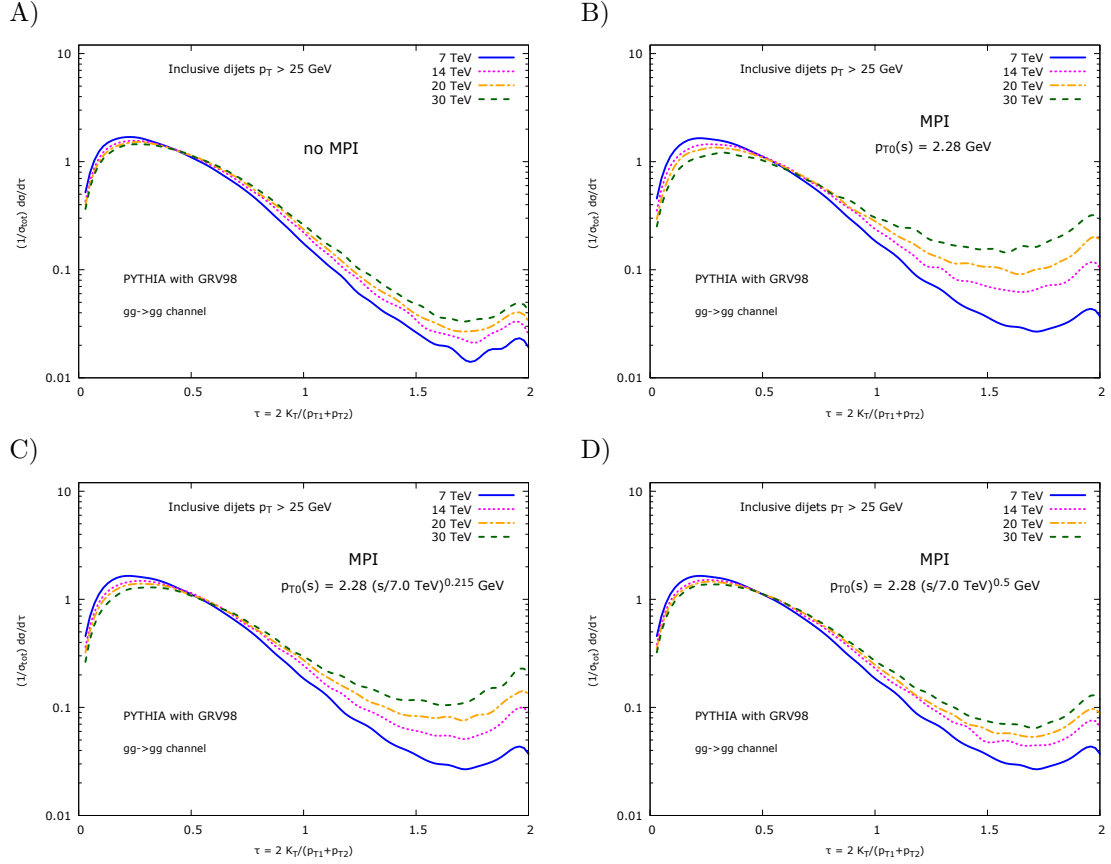
Figure 10: Spectra of the variable $\tau = 2K_T/(p_{T1} + p_{T2})$ in pythia with parton showers, no hadronization and with several choices of MPI model parameters. A) MPI is switched off, B) the $p_{T0}(S) = \text{const.}$, C) the standard choice of (13), D) the choice (13) but with the exponent approximately as twice as big.
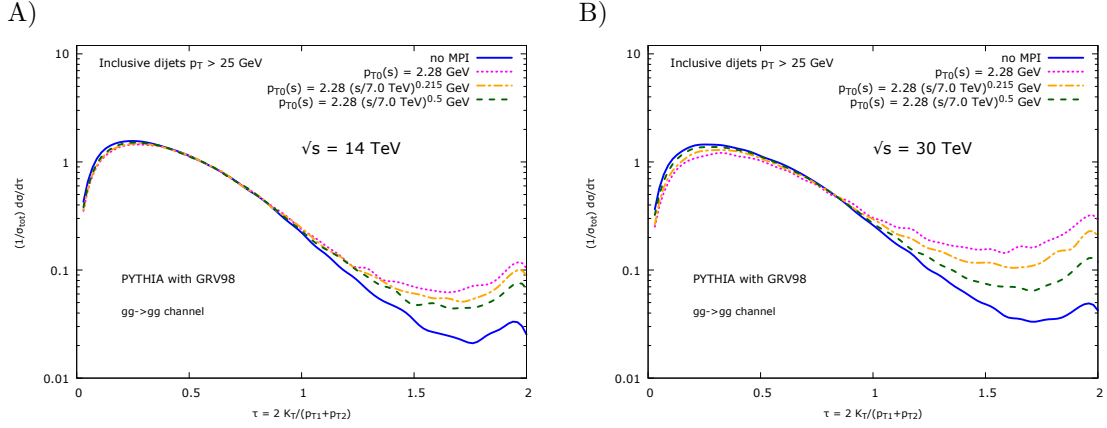
Figure 11: Similar to Fig. 10 but here we compare calculations with different MPI model parameter and fixed CM energy: A) 14 TeV, B) 30 TeV.
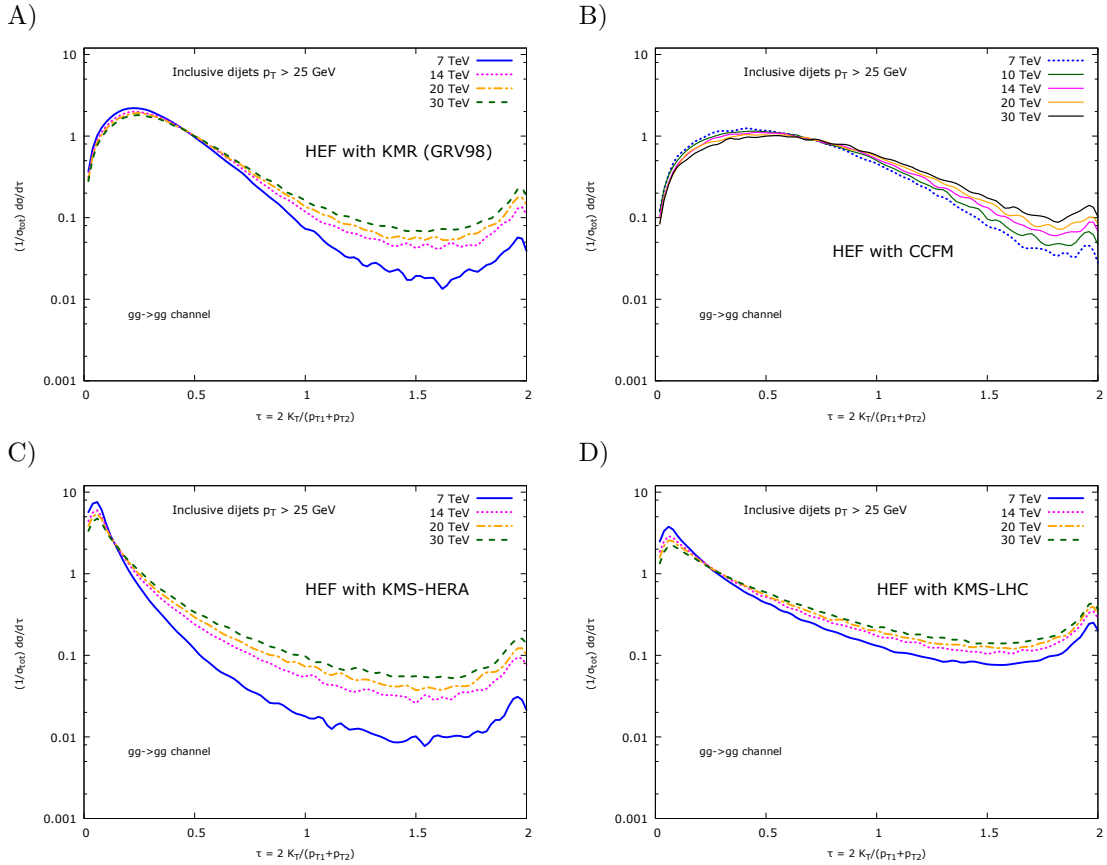

Figure 12: Spectra of the variable $\tau = 2K_T/(p_{T1} + p_{T2})$ in HEF with various UGDs: A) KMR with GRV98, B) the CCFM, C) the KMS-HERA, D) the KMS-LHC.
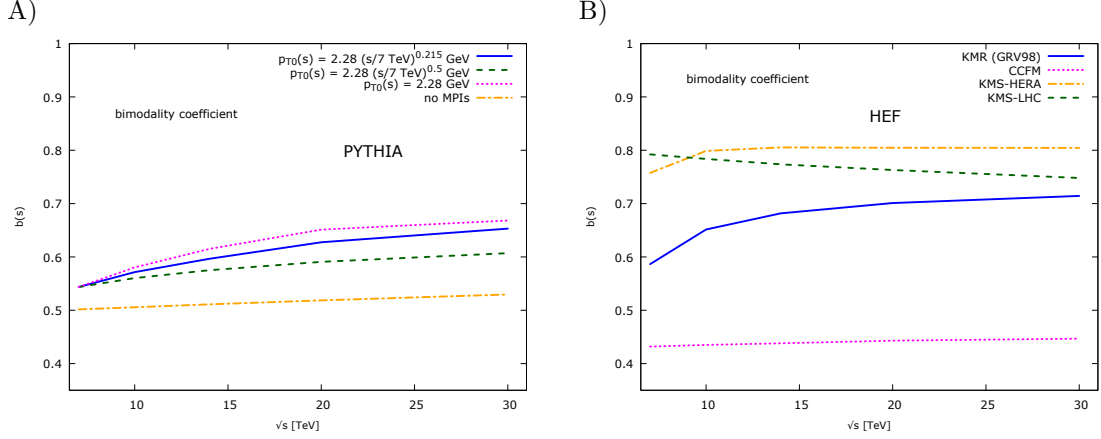
A)   B)

Figure 13: The bimodality coefficient defined in (44) for various approaches as a function of energy. A) pythia with different minijet suppression , B) HEF with various UGDs.

coefficient defined as

$$b = \frac{\gamma^2 + 1}{\kappa} \, , \tag{44}$$

where the skewness γ and the kurtosis κ are defined as

$$\gamma = \frac{\mu_3}{\sigma^3} \, , \quad \kappa = \frac{\mu_4}{\sigma^4} \, , \tag{45}$$

with μ_n being the n-th central moment and σ the standard deviation. We calculate b as a function of energy in Fig. 13A. We see that the bimodality coefficient reflects (to some extent) the energy dependence of the minijets contribution. When there are no MPIs the coefficient is perfectly linear with energy. When we switch on MPIs b jumps to a higher value and then the increase is dictated by the amount of suppression of minijets. Thus we may conclude, that the bimodality coefficient of the normalized spectra in τ is a reasonable measure of the minijet contribution as a function of energy *when a hard process is present.*

Let us now turn to HEF and make a similar analysis. First we calculate the spectra in τ shown in Fig. 12. Interestingly, we see that these spectra also feature the bimodal character. There is no explicit parton shower in HEF, however the transverse momentum dependent gluons with exact off-shell kinematics render an equivalent of the initial state parton shower (see e.g. [61, 85]). As we discussed for the pythia case, the initial state shower contributes significantly to this region. We saw however that this contribution alone has different energy dependence than when MPIs are added. It will thus interesting to study the energy dependence of the second peak in HEF and compare it with pythia. The results for the τ distribution are shown in Fig. 12. We see that KMR with GRV98 (Fig. 12A) produce superficially similar spectra to those of pythia with MPIs. The CCFM (Fig. 12B) looks more flat with the second peak only very slowly varying with energy. The KMS distribution which does not have the hard scale evolution (i.e. the Sudakov resummation) produce very different shapes. They are much more peaked near $\tau = 0$ (Figs. 12C-D). Spectra for both versions of KMS also differ considerably with respect to the second peak. To compare the energy evolution of the second peak let us now extract the bimodality coefficient from these spectra. The result is presented in Fig. 13B. First, we see that the normalizations vary significantly for different models. This is because the

normalization is sensitive to the first peak, which is different across models. Second, looking at the energy dependence, we see that the KMR with GRV98 has a similar (but not the same) tendency to pythia with MPIs and the suppression parameter $p_{T0}(S) = $ const. The rise with energy is slightly slower, but not as slow as the model (13). It is better seen in Fig. 14 where we collect the pythia results with only extreme settings for clarity and some of the HEF results. In this plot we normalize the bimodality coefficient by its value at 7 TeV to compare the energy dependence. The conclusion from this plot is as follows. The HEF can render power corrections which definitely can show similar energy evolution to the one from MPIs in the event generator (due to the evolution of $p_T(S)$). Here it is satisfied by KMR and KMS-HERA UGDs. It seems however that the energy dependence they give flattens earlier than pythia minijet models. The initial rise is also more rapid.

There are several comments in order. First, the bimodality coefficient from pythia models depends on the jet radius R as does the calculated τ distribution for large τ. It is clear that by decreasing the jet radius we will reconstruct more jets which will eventually start to balance each other. This sensitivity of large τ to R is a natural feature. In this regime the dijets are accompanied by a large 'underlying event' activity. From LHC data [93] it is known that the underlying event observables are sensitive to R. The sensitivity mechanism of τ distribution on R will become more clear from the discussion below. Second comment concerns the chosen rapidity coverage, namely $|\eta| < 4$. In pythia without MPIs the recoiling system for large τ most probably consists from a hard jet (or jets) which lie outside the chosen rapidity window. Thus one may wonder how the results depend on the rapidity coverage. We verified that there is no change in τ distributions (both with and without MPIs) for the rapidity window widths between $|\eta| < 2$ and $|\eta| < 5$. In HEF the dijet imbalance is produced by the emissions which are hidden in the k_T dependent UGDs. The standard small-x evolution equations do not order emissions in k_T, thus the large imbalance can be caused by either several softer emissions or one very hard. By definition, these are unresolved, untagged, emissions. Moreover, they are further away in rapidity than the hard process. In evolution equations which mix the evolution in hard scale and x the situation is more complicated, but there is always a possibility to have a harder jet outside the acceptance. Clearly, the detailed structure of the recoiling system cannot be fully explored by solely studying the inclusive quantity like the production of two dijets. While pythia being the full event generator can provide such information, it is impossible to resolve these emissions on the level of inclusive HEF factorization used in this work. In order to answer this question a full event generator based on the HEF factorization with un-ordered emissions (in k_T) and exact energy momentum conservation would be needed. Therefore, further detailed studies of this contribution are necessary.

To see more directly how the large K_T disbalance can be created due to MPIs, we display in Fig. 15 several events in (ϕ, η, p_T) space obtained from pythia with MPI and parton showers. We have traced the origin of the final state particles that later form the jets; particles originating in different hard collision are denoted using different colors. The resulting jets are displayed as cones with radius $R = 0.5$. The two top plots present two events with small disbalance relative to the hard scale (small τ). We see that the jets are reconstructed from the particles originating in the same hard collision. The bottom plots show two events which contribute to large disbalance to hard scale ratio τ, thus to power corrections. We see that the leading jets are reconstructed from final state partons originating from different hard collisions. Moreover, we see that a mixture of partons from different hard collisions may enter a jet.

Let us now make some comments on the energy dependence of the power corrections from UGDs other then KMR, that is undergoing the BFKL evolution and its extensions. From Fig. 14 it seems that they give much weaker energy dependence than Sudakov-based KMR
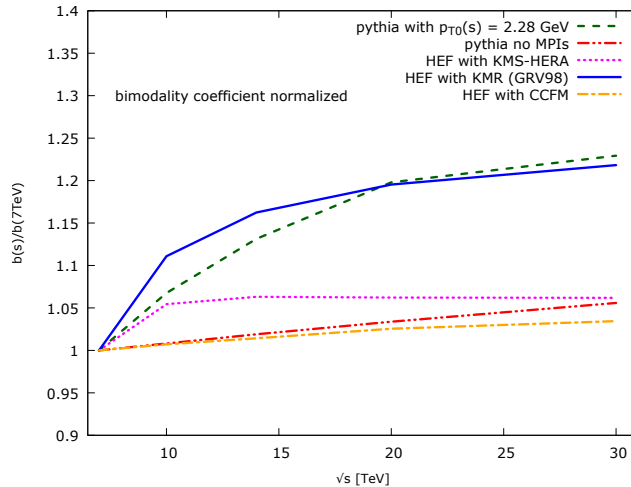
Figure 14: Comparision of energy dependence of the bimodality coefficient normalized to the value at 7 TeV for some of the curves from Fig. 13A-B.

approach. In particular the CCFM gluon distribution gives the behaviour of power corrections as if there were no MPIs. This is interesting and may be connected to the particular way the emissions are ordered, namely it is less probable in CCFM to emit a hard gluon far away in rapidity. Let us stress however, that different CCFM sets differ considerably depending on the particular implementation (we are not concerned in comparing various CCFM distributions in this paper). Moreover, all BFKL-based gluons have been fitted to experimental data on the structure functions in Deep Inelastic Scattering. This process is dominated by small k_T and thus the large k_T tails of these distributions are burdened with rather sizeable errors. It is thus important to keep in mind these restrictions.
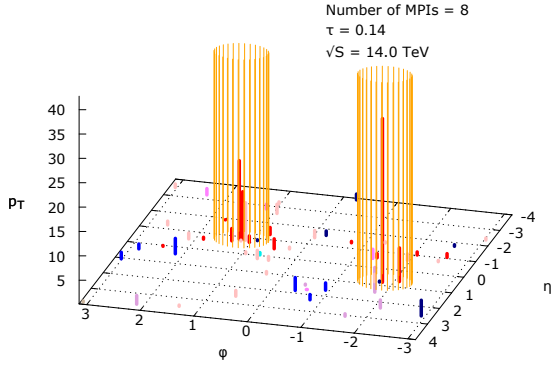
6   Summary and conclusions

Our work can be summarized as follows. We have performed a comprehensive analysis of the minijet cross section and its crucial component – the p_T cutoff. Despite the fact that in event generators minijets are described by the collinear formula, the kinematic domain ventures out of the leading power approximation. Therefore we attempted to explain the cutoff using various forms of k_T-factorization for inclusive dijet production: the High Energy Factorization (HEF) with two off-shell gluons in the initial state and an extension of the Dokshitzer-Dyakonov-Troyan formula beyond the leading power (IDDT). Both approaches involve unintegrated gluon distributions (UGD) which inject nonzero transverse momentum into the hard process and thus there is a potential mechanism for a dynamical cutoff on small p_T.
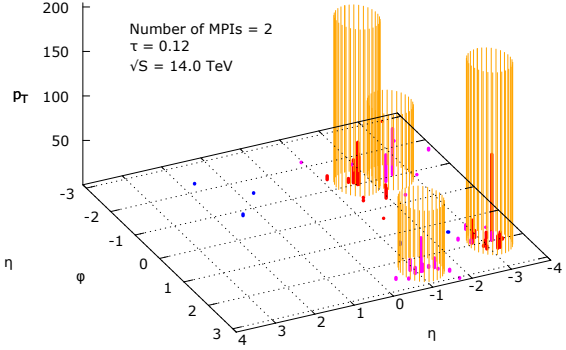
We have performed two analyses: (i) direct calculations of p_T spectra in the low-p_T region ($p_T > 2 \, \text{GeV}$) to see if the cutoff is generated, (ii) calculations for relatively hard inclusive dijets with $p_T > 25 \, \text{GeV}$ and analysis of subleading effects in search for a patterns of minijets.

As far as the direct study (i) is concerned we find that the suppression which is generated is small and has a 'kinematic' origin and thus the opposite energy dependence than in the MC models. It is in fact something one should expect as the leading contribution to the cross section
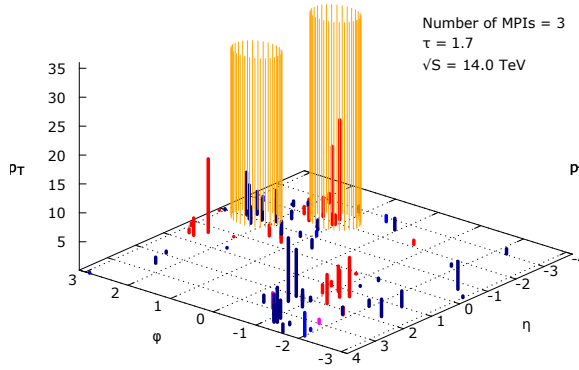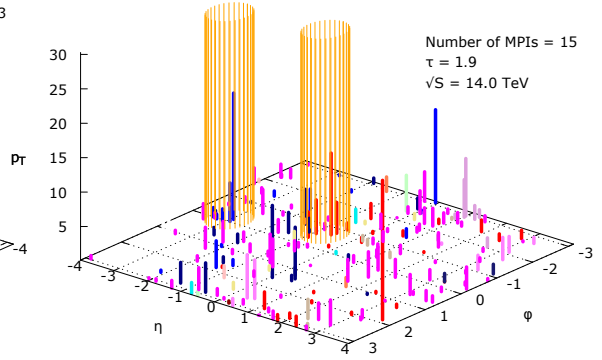
28

A)

Number of MPIs = 8
τ = 0.14
√S = 14.0 TeV

B)

Number of MPIs = 2
τ = 0.12
√S = 14.0 TeV

C)

Number of MPIs = 3
τ = 1.7
√S = 14.0 TeV

D)

Number of MPIs = 15
τ = 1.9
√S = 14.0 TeV

Figure 15: Events in (ϕ, η, p_T) space from pythia where the final state particles and their MPI origin are shown. Particles originating in various hard processeses (above certain p_T threshold) are denoted using different colors. The reconstructed leading jets are symbolically represented by cylinders with radius 0.5. The beam remnants are also displayed. The top row (A-B) represents events with small relative momentum disbalance τ (relative to the hard scale). The bottom row (C-D) represent events where the relative disbalance τ is large. We see that the leading jets originate from different subprocesses here.

in HEF/IDDT with $2 \to 2$ hard process comes from the very small internal transverse momenta. The results are similar to the ones obtained from pythia when the 'hard QCD' block is used.

In the study (ii) we use differential cross section in a variable τ defined to be the ratio of dijet disbalance to the average p_T. We observe, that when it is calculated in pythia with MPIs it has a bimodal character with one bump located close to $\tau \sim 0$ and the second bump (much smaller) located close to $\tau \sim 2$. The second bump is sensitive to the p_T cutoff in MPI model. The same observable calculated within HEF reveals similar feature. We investigated the energy dependence of the bimodality coefficient b which characterizes the relative magnitude of the two peaks. We find that the energy dependence of b calculated from pythia resembles the energy evolution of the p_T cutoff in MPI model. Thus by studying b in HEF we could obtain information about minijets constituting emissions which lead to the dijet disbalance. We found that the UGD constructed according to the prescription which uses collinear gluon PDF and Sudakov form factor (proposed by Kimber, Martin and Ryskin and before that indirectly by Diakonov, Dokshitzer and Troyan) produces minijets which are only slightly suppressed with CM energy (for large energies). The UGDs with explicit BFKL kernel present give stronger suppression. None of the models recovers exactly the minijet suppression from the pythia event generator.

Let us stress that we did not intend to compare pythia and HEF. Conversely, we have used pythia to give a possible interpretation to power corrections present in the HEF approach. The latter is by definition an inclusive formulation and certain effects are hidden, or, broadly speaking, parametrized by the k_T dependent gluon distributions. One has to keep in mind that this was done neglecting the details of the recoil system present outside the acceptance region.

We note that while it is practically impossible to measure the minijets directly, where by 'directly' we mean a measurement of p_T spectrum around $p_T \sim 2\,\mathrm{GeV}$ with reconstructed jets (although charged particle jets could be possible), our study (ii) is feasible with the current detectors operating at the LHC. This could supplement the measurements of underlying event (e.g. [94]) as a main source of restricting MPI model parameters [95].

In the present work we did not discuss the gluon saturation [11] issues. It is clear that at some point for very high energies the nonlinear effects in the gluon density should come into play, especially at small p_T. In a naive study, where one would just use UGD with nonlinear evolution of the Balitsky-Kovchegov type [96, 97] the situation would not change significantly, unless large saturation scale $Q_s \sim p_T$ is used. The point is however, that the HEF is not correct in the saturation domain and more complicated approach involving several UGDs is needed [59, 98]. Whether such improved factorization can generate a sizeable cutoff with the right energy dependence is still open, especially since the problem with the cutoff persists for large impact parameters where gluon densities are not too large [6, 7].

One of the important practical outcomes of the present work is the observation that the naive mixing HEF and double parton scattering mechanism can lead to the double counting. The latter is based on the leading twist factorization and using it by simply replacing the collinear expressions by k_T factorized expressions may double count in the region sensitive to large gluon transverse momenta. Whether this happens depends on particular evolution used for the unintegrated gluon distribution.

In other words, we have demonstrated that the HEF can imitate the MPIs effect in the region of large relative dijet momentum imbalance, depending on the choice of the unintegrated gluon distributions. We did this via numeric simulations of relevant observables in both approaches and comparing them. It would be interesting to do a detailed analytical study of power corrections in both approaches. This is beyond the present work and is left for a future study.

Acknowledgments

References

[1] J. Collins, *Foundations of perturbative QCD*, vol. 32. Cambridge Univ. Press, 2011.

[2] I. Sarcevic, S. D. Ellis and P. Carruthers, *QCD minijet cross sections*, Phys. Rev. D **40** (sep, 1989) 1446–1452.

[3] T. Sjöstrand, S. Mrenna and P. Skands, *PYTHIA 6.4 physics and manual*, J. High Energy Phys. **2006** (may, 2006) 026–026, [hep-ph/0603175].

[4] M. Bähr, S. Gieseke, M. A. Gigg, D. Grellscheid, K. Hamilton, O. Latunde-Dada et al., *Herwig++ physics and manual*, Eur. Phys. J. C **58** (dec, 2008) 639–707, [0803.0883].

[5] T. Sjöstrand and M. van Zijl, *A multiple-interaction model for the event structure in hadron collisions*, Phys. Rev. D **36** (oct, 1987) 2019–2041.

[6] T. C. Rogers, A. M. Staśto and M. I. Strikman, *Unitarity constraints on semihard jet production in impact parameter space*, Phys. Rev. D **77** (jun, 2008) 114009.

[7] T. C. Rogers and M. Strikman, *Multiple hard partonic collisions with correlations in proton-proton scattering*, Phys. Rev. D **81** (jan, 2010) 016013.

[8] B. Blok, Y. Dokshitzer, L. Frankfurt and M. Strikman, *Four-jet production at LHC and Tevatron in QCD*, Phys. Rev. D **83** (apr, 2011) 071501, [1009.2714].

[9] M. Diehl, D. Ostermeier and A. Schäfer, *Elements of a theory for multiparton interactions in QCD*, J. High Energy Phys. **2012** (mar, 2012) 89, [1111.0910].

[10] M. Diehl, J. R. Gaunt, D. Ostermeier, P. Plößl and A. Schäfer, *Cancellation of Glauber gluon exchange in the double Drell-Yan process*, J. High Energy Phys. **2016** (jan, 2016) 76.

[11] L. V. Gribov, E. M. Levin and M. G. Ryskin, *Semihard processes in QCD*, Phys. Rep. **100** (nov, 1983) 1–150.

[12] S. Catani, M. Ciafaloni and F. Hautmann, *High energy factorization and small-x heavy flavour production*, Nucl. Phys. B **366** (nov, 1991) 135–188.

[13] S. Catani, M. Ciafaloni and F. Hautmann, *Gluon contributions to small χ heavy flavour production*, Phys. Lett. B **242** (may, 1990) 97–102.

[14] S. Catani and F. Hautmann, *High-energy factorization and small-x deep inelastic scattering beyond leading order*, Nucl. Phys. B **427** (oct, 1994) 475–524, [hep-ph/9405388].

[15] J. Collins and R. Ellis, *Heavy-quark production in very high energy hadron collisions*, Nucl. Phys. B **360** (aug, 1991) 3–30.

[16] V. Fadin, E. Kuraev and L. Lipatov, *On the pomeranchuk singularity in asymptotically free theories*, *Phys. Lett. B* **60** (dec, 1975) 50–52.

[17] E. A. Kuraev, L. N. Lipatov and V. S. Fadin, *The Pomeranchuk Singularity in Nonabelian Gauge Theories*, *Sov.Phys.JETP* **45** (1977) 199–204.

[18] I. I. Balitsky and L. N. Lipatov, *The Pomeranchuk Singularity in Quantum Chromodynamics*, *Sov.J.Nucl.Phys.* **28** (1978) 822–829.

[19] M. Kimber, A. Martin and M. Ryskin, *Unintegrated parton distributions and prompt photon hadroproduction*, *Eur. Phys. J. C* **12** (feb, 2000) 655–661, [`hep-ph/9911379`].

[20] M. A. Kimber, A. D. Martin and M. G. Ryskin, *Unintegrated parton distributions*, *Phys. Rev. D* **63** (may, 2001) 114027, [`hep-ph/0101348`].

[21] G. Parisi and R. Petronzio, *Small transverse momentum distributions in hard processes*, *Nucl. Phys. B* **154** (aug, 1979) 427–440.

[22] A. Grau, G. Pancheri and Y. N. Srivastava, *Hadronic total cross sections through soft gluon summation in impact parameter space*, *Phys. Rev. D* **60** (nov, 1999) 114020.

[23] D. A. Fagundes, A. Grau, G. Pancheri, Y. N. Srivastava and O. Shekhovtsova, *Soft edge of hadron scattering and minijet models for the total and inelastic pp cross sections at LHC and beyond*, *Phys. Rev. D* **91** (jun, 2015) 114011.

[24] G. Gustafson and G. Miu, *Minijets and transverse energy flow in high energy collisions*, *Phys. Rev. D* **63** (2001) 034004.

[25] H. Kharraziha and L. Lönnblad, *The linked dipole chain Monte Carlo*, *J. High Energy Phys.* **1998** (mar, 1998) 006–006.

[26] G. Gustafson, L. Lönnblad and G. Miu, *Hadronic collisions in the linked dipole chain model*, *Phys. Rev. D* **67** (feb, 2003) 034020.

[27] M. Ciafaloni, *Coherence Effects in Initial Jets at Small q^{**2} / s*, *Nucl. Phys. B* **296** (jan, 1988) 49–74.

[28] S. Catani, F. Fiorani and G. Marchesini, *QCD coherence in initial state radiation*, *Phys. Lett. B* **234** (jan, 1990) 339–345.

[29] S. Catani, F. Fiorani and G. Marchesini, *Small-x behaviour of initial state radiation in perturbative QCD*, *Nucl. Phys. B* **336** (may, 1990) 18–85.

[30] B. Andersson, G. Gustafson and J. Samuelsson, *The linked dipole chain model for DIS*, *Nucl. Phys. B* **467** (1996) 443–476.

[31] Y. Dokshitzer, D. Dyakonov and S. Troyan, *Hard processes in quantum chromodynamics*, *Phys. Rep.* **58** (feb, 1980) 269–395.

[32] V. V. Sudakov, *Vertex parts at very high-energies in quantum electrodynamics*, *Sov.Phys.JETP* **3** (1956) 65–71.

[33] M. Glück, E. Reya and A. Vogt, *Dynamical parton distributions revisited*, *Eur. Phys. J. C5* (1998) 461–470.

[34] Y. Dokshitzer, D. Dyakonov and S. Troyan, *Hard semi-inclusive processes in QCD*, *Phys. Lett. B* **78** (sep, 1978) 290–294.

[35] G. Curci, M. Greco and Y. Srivastava, *QCD jets from coherent states*, *Nucl. Phys. B* **159** (nov, 1979) 451–468.

[36] P. Chiappetta and M. Greco, *Transverse momentum distributions for Drell-Yan pairs in QCD*, *Phys. Lett. B* **106** (nov, 1981) 219–223.

[37] J. Collins, D. E. Soper and G. Sterman, *Transverse momentum distribution in Drell-Yan pair and W and Z boson production*, *Nucl. Phys. B* **250** (jan, 1985) 199–224.

[38] X. Ji, J.-P. Ma and F. Yuan, *QCD factorization for semi-inclusive deep-inelastic scattering at low transverse momentum*, *Phys. Rev. D* **71** (feb, 2005) 034005, [`0404183`].

[39] T. C. Rogers and P. J. Mulders, *No generalized transverse momentum dependent factorization in the hadroproduction of high transverse momentum hadrons*, *Phys. Rev. D* **81** (may, 2010) 094006, [`1001.2977`].

[40] P. Sun, C. P. Yuan and F. Yuan, *Transverse momentum resummation for dijet correlation in hadronic collisions*, *Phys. Rev. D - Part. Fields, Gravit. Cosmol.* **92** (2015) 1–33, [`arXiv:1506.06170v1`].

[41] R. L. Jaffe and M. Soldate, *Twist-4 effects in electroproduction: Canonical operators and coefficient functions*, *Phys. Rev. D* **26** (jul, 1982) 49–68.

[42] R. Ellis, W. Furmański and R. Petronzio, *Power corrections to the parton model in QCD*, *Nucl. Phys. B* **207** (nov, 1982) 1–14.

[43] I. Anikin, D. Ivanov, B. Pire, L. Szymanowski and S. Wallon, *QCD factorization of exclusive processes beyond leading twist: impact factor with twist three accuracy*, *Nucl. Phys. B* **828** (mar, 2010) 1–68.

[44] V. M. Braun and A. N. Manashov, *Operator product expansion in QCD in off-forward kinematics: separation of kinematic and dynamical contributions*, *J. High Energy Phys.* **2012** (jan, 2012) 85.

[45] G. Altarelli, G. Parisi and R. Petronzio, *Transverse momentum in Drell-Yan processes*, *Phys. Lett. B* **76** (jun, 1978) 351–355.

[46] G. Altarelli, R. Ellis, M. Greco and G. Martinelli, *Vector boson production at colliders: A theoretical reappraisal*, *Nucl. Phys. B* **246** (nov, 1984) 12–44.

[47] J. C. Collins, *Hard-scattering factorization with heavy quarks: A general treatment*, *Phys. Rev. D* **58** (sep, 1998) 094002, [`9806259`].

[48] P. Kotko and W. Slominski, *General mass scheme for jet production in DIS*, *Phys. Rev. D* **86** (nov, 2012) 094008, [`1206.4024`].

[49] R. Doria, J. Frenkel and J. Taylor, *Counter-example to non-abelian Bloch-Nordsieck conjecture*, *Nucl. Phys. B* **168** (may, 1980) 93–110.

[50] A. van Hameren, K. Kutak and T. Salwa, *Scattering amplitudes with off-shell quarks*, *Phys. Lett. B* **727** (nov, 2013) 226–233, [`1308.2861`].

[51] K. Kutak, R. Maciula, M. Serino, A. Szczurek and A. van Hameren, *Four-jet production in single- and double-parton scattering within high-energy factorization*, J. High Energy Phys. **2016** (apr, 2016) 175.

[52] A. Leonidov and D. Ostrovsky, *Angular and momentum asymmetry in particle production at high energies*, Phys. Rev. D **62** (oct, 2000) 094009, [hep-ph/9905496].

[53] M. Deak, F. Hautmann, H. Jung and K. Kutak, *Forward jet production at the Large Hadron Collider*, J. High Energy Phys. **2009** (sep, 2009) 121–121, [0908.0538].

[54] M. Deak, F. Hautmann, H. Jung and K. Kutak, *Forward-Central Jet Correlations at the Large Hadron Collider*, 1012.6037.

[55] M. Deak, F. Hautmann, H. Jung and K. Kutak, *Forward jets and energy flow in hadronic collisions*, Eur. Phys. J. C **72** (apr, 2012) 1982, [1112.6354].

[56] J.-P. Blaizot, F. Gelis and R. Venugopalan, *High energy pA collisions in the color glass condensate approach I: gluon production and the Cronin effect*, Nucl. Phys. A **743** (oct, 2004) 13–56, [hep-ph/0402256].

[57] A. Dumitru, A. Hayashigaki and J. Jalilian-Marian, *The color glass condensate and hadron production in the forward region*, Nucl. Phys. A **765** (feb, 2006) 464–482, [hep-ph/0506308].

[58] E. Iancu and J. Laidet, *Gluon splitting in a shockwave*, Nucl. Phys. A **916** (oct, 2013) 48–78.

[59] P. Kotko, K. Kutak, C. Marquet, E. Petreska, S. Sapeta and A. van Hameren, *Improved TMD factorization for forward dijet production in dilute-dense hadronic collisions*, J. High Energy Phys. **2015** (sep, 2015) 106, [1503.03421].

[60] A. van Hameren, P. Kotko and K. Kutak, *Three-jet production and gluon saturation effects in p-Pb collisions within high-energy factorization*, Phys. Rev. D **88** (nov, 2013) 094001, [1308.0452].

[61] A. van Hameren, P. Kotko, K. Kutak and S. Sapeta, *Small-x dynamics in forward-central dijet correlations at the LHC*, Phys. Lett. B **737** (oct, 2014) 335–340, [1404.6204].

[62] A. van Hameren, P. Kotko, K. Kutak, C. Marquet and S. Sapeta, *Saturation effects in forward-forward dijet production in p+Pb collisions*, Phys. Rev. D **89** (may, 2014) 094014, [1402.5065].

[63] A. van Hameren, P. Kotko and K. Kutak, *Resummation effects in the forward production of Z0 + jet at the LHC*, Phys. Rev. D **92** (sep, 2015) 054007.

[64] A. Van Hameren, P. Kotko and K. Kutak, *Helicity amplitudes for high-energy scattering*, J. High Energy Phys. **2013** (2013) .

[65] L. Lipatov, *Gauge invariant effective action for high energy processes in QCD*, Nucl. Phys. B **452** (oct, 1995) 369–397, [hep-ph/9502308].

[66] E. Antonov, I. Cherednikov, E. Kuraev and L. Lipatov, *Feynman rules for effective Regge action*, Nucl. Phys. B **721** (aug, 2005) 111–135, [0411185].

[67] P. Kotko, *Wilson lines and gauge invariant off-shell amplitudes*, *J. High Energy Phys.* **2014** (jul, 2014) 128, [`1403.4824`].

[68] C. Cruz-Santiago, P. Kotko and A. M. Staśto, *Recursion relations for multi-gluon off-shell amplitudes on the light-front and Wilson lines*, *Nucl. Phys. B* **895** (2015) 132–160.

[69] P. Kotko, M. Serino and A. M. Stasto, *Off-shell amplitudes as boundary integrals of analytically continued Wilson line slope*, `1601.02953`.

[70] R. Britto, F. Cachazo and B. Feng, *New recursion relations for tree amplitudes of gluons*, *Nucl. Phys. B* **715** (may, 2005) 499–522, [`hep-th/0412308`].

[71] R. Britto, F. Cachazo, B. Feng and E. Witten, *Direct Proof of the Tree-Level Scattering Amplitude Recursion Relation in Yang-Mills Theory*, *Phys. Rev. Lett.* **94** (may, 2005) 181602, [`hep-th/0501052`].

[72] A. Van Hameren, *BCFW recursion for off-shell gluons*, *J. High Energy Phys.* **2014** (jul, 2014) 138, [`1404.7818`].

[73] A. van Hameren and M. Serino, *BCFW recursion for TMD parton scattering*, *J. High Energy Phys.* **2015** (jul, 2015) 10.

[74] A. Van Hameren, P. Kotko and K. Kutak, *Multi-gluon helicity amplitudes with one off-shell leg within high energy factorization*, *J. High Energy Phys.* **2012** (2012) , [`1207.3332`].

[75] M. A. Nefedov, V. A. Saleev and A. V. Shipilova, *Dijet azimuthal decorrelations at the LHC in the parton Reggeization approach*, *Phys. Rev. D* **87** (may, 2013) 094030.

[76] V. A. Saleev, *Diphoton production at the Tevatron in the quasi-multi-Regge-kinematic approach*, *Phys. Rev. D* **80** (dec, 2009) 114016, [`0911.5517`].

[77] B. A. Kniehl, V. A. Saleev, A. V. Shipilova and E. V. Yatsenko, *Single jet and prompt-photon inclusive production with multi-Regge kinematics: From Tevatron to LHC*, *Phys. Rev. D* **84** (oct, 2011) 074017, [`1107.1462`].

[78] R. Maciuła, R. Pasechnik and A. Szczurek, *Central exclusive quark-antiquark dijet and standard model Higgs boson production in proton-(anti)proton collisions*, *Phys. Rev. D* **83** (jun, 2011) 114034.

[79] V. A. Saleev and A. V. Shipilova, *Inclusive b -jet and b bÂŕ-dijet production at the LHC via Reggeized gluons*, *Phys. Rev. D* **86** (aug, 2012) 034032, [`1201.4640`].

[80] R. Maciuła and A. Szczurek, *Open charm production at the LHC: kT-factorization approach*, *Phys. Rev. D* **87** (may, 2013) 094022.

[81] R. Maciuła and A. Szczurek, *Production of c cbar c cbar in double-parton scattering within the kT-factorization approach: Meson-meson correlations*, *Phys. Rev. D* **87** (apr, 2013) 074039.

[82] M. L. Mangano and S. J. Parke, *Multi-parton amplitudes in gauge theories*, *Phys. Rep.* **200** (feb, 1991) 301–367, [`hep-th/0509223`].

[83] P. Kotko, *LxJet program*, `http://annapurna.ifj.edu.pl/~pkotko/LxJet.html`, 2013.

[84] S. Jadach, *Foam: A general-purpose cellular Monte Carlo event generator*, *Comput. Phys. Commun.* **152** (apr, 2003) 55–100, [0203033].

[85] M. Bury, M. Deak, K. Kutak and S. Sapeta, *Single and double inclusive forward jet production at the LHC at $\sqrt{s} = 7$ and 13 TeV*, *ArXiv:1604.01305* (apr, 2016) , [1604.01305].

[86] J. Kwiecinski, A. D. Martin and A. M. Stasto, *Unified BFKL and Gribov-Lipatov-Altarelli-Parisi description of F2 data*, *Phys. Rev. D* **56** (oct, 1997) 3991–4006, [hep-ph/9703445].

[87] K. Kutak and S. Sapeta, *Gluon saturation in dijet production in p-Pb collisions at the Large Hadron Collider*, *Phys. Rev. D* **86** (nov, 2012) 094043, [1205.5035].

[88] P. Kotko, W. Słomiński and D. Toton, *Unintegrated Gluon Distributions for Forward Jets at the LHC*, *Acta Phys. Pol. B* **46** (apr, 2015) 1527, [1504.00823].

[89] F. Hautmann, H. Jung, M. Krämer, P. J. Mulders, E. R. Nocera, T. C. Rogers et al., *TMDlib and TMDplotter: library and plotting tools for transverse-momentum-dependent parton distributions*, *Eur. Phys. J. C* **74** (dec, 2014) 3220.

[90] F. Hautmann, H. Jung and S. T. Monfared, *The CCFM uPDF evolution uPDFevolv Version 1.0.00*, *Eur. Phys. J. C* **74** (oct, 2014) 3082, [1407.5935].

[91] J. Kwiecinski, *Unintegrated gluon distributions from the transverse coordinate representation of the CCFM equation in the single loop approximation*, *Acta Phys.Polon.* **B33** (2002) 1809–1822.

[92] V. Abramovsky, V. Gribov and O. Kancheli, *Character of Inclusive Spectra and Fluctuations Produced in Inelastic Processes by Multi - Pomeron Exchange*, *Sov.J.Nucl.Phys.* **18** (1973) 595–616.

[93] CMS Collaboration, *Underlying event characteristics and their dependence on jet size of charged-particle jet events in pp collisions at $\sqrt{s} = 7$ TeV with the ATLAS detector*, *Phys.Rev.* **D86** (2012) 072004.

[94] CMS Collaboration, *Underlying Event Measurements with Leading Particles and Jets in pp collisions at $\sqrt{s} = 13$ TeV*, *CMS-PAS-FSQ-15-007* (2015) .

[95] M. H. Seymour and A. Siódmok, *Constraining MPI models using σ eff and recent Tevatron and LHC Underlying Event data*, *J. High Energy Phys.* **2013** (oct, 2013) 113, [arXiv:1307.5015v2].

[96] I. Balitsky, *Operator expansion for high-energy scattering*, *Nucl. Phys. B* **463** (1996) 99–157, [hep-ph/9509348].

[97] Y. V. Kovchegov, *Small- x F 2 structure function of a nucleus including multiple Pomeron exchanges*, *Phys. Rev. D* **60** (jun, 1999) 034008, [hep-ph/9901281].

[98] A. van Hameren, P. Kotko, K. Kutak, C. Marquet, E. Petreska and S. Sapeta, *Forward di-jet production in p+Pb collisions in the small-x improved TMD factorization framework*, 1607.03121.

[99] D. Binosi and L. Theußl, *JaxoDraw: A graphical user interface for drawing Feynman diagrams, Comput. Phys. Commun.* **161** (aug, 2004) 76–86, [hep-ph/0309015].